NASA TECHNICAL NOTE

NASA TN D-3227

NASA TN D-3227

WEIGHT STUDY OF PARTIALLY SEGMENTED DIRECT-CONDENSING RADIATORS FOR LARGE SPACE POWER SYSTEMS

by Roy L. Johnsen

Lewis Research Center
Cleveland, Ohio

NATIONAL AERONAUTICS AND SPACE ADMINISTRATION • WASHINGTON, D. C. • JANUARY 1966

NASA TN D-3227

WEIGHT STUDY OF PARTIALLY SEGMENTED DIRECT-CONDENSING RADIATORS FOR LARGE SPACE POWER SYSTEMS

By Roy L. Johnsen

Lewis Research Center
Cleveland, Ohio

NATIONAL AERONAUTICS AND SPACE ADMINISTRATION

For sale by the Clearinghouse for Federal Scientific and Technical Information
Springfield, Virginia 22151 – Price $2.00

WEIGHT STUDY OF PARTIALLY SEGMENTED DIRECT-CONDENSING RADIATORS FOR LARGE SPACE POWER SYSTEMS

by Roy L. Johnsen

Lewis Research Center

SUMMARY

An analytical investigation has been performed to provide an insight into the weight increase of a direct-condensing radiator for a potassium Rankine cycle space power system as the system size was increased from 1 to 10 megawatts electric while holding constant the component efficiencies and all cycle temperatures and pressures.

The largest single contributor to the radiator weight is the armor necessary to protect fluid passages from meteoroid puncture. The two most important factors affecting armor thickness are the meteoroid population estimate and the radiator design survival probability. Design survival probabilities of 0.9, 0.95, and 0.99 were used with a high meteoroid population estimate, Whipple's (1961), and a low estimate, Watson's (1956), for 1, 10, 20, and 100 radiator segments.

The radiator weight is sharply influenced by the meteoroid flux estimate and the design survival probability. For the unsegmented case, using Watson's (1956) flux estimate, the radiator weight ranged from 1.5 to 3 pounds per kilowatt electric for the 1- to 10-megawatt power range for a 0.9 radiator design survival probability, and 2.5 to 6 pounds per kilowatt for a 0.99 design survival probability. When Whipple's (1961) flux estimate was used, the radiator weight ranged from 7 to 17 pounds per kilowatt for a 0.9 design survival probability and from 16 to 42 pounds per kilowatt for a 0.99 design survival probability.

Segmentation of the radiator provided significant weight savings over the unsegmented radiator, especially when high survival probabilities were demanded. Generally the weight advantages of segmentation increased with increases in system power level, design survival probability, number of segments, and severity of the meteoroid flux estimate. When Whipple's (1961) meteoroid flux estimate and a 0.99 design survival probability for a 10-megawatt system were used, the radiator with 100 segments was about one-fourth the weight of an unsegmented radiator.

With segmentation the ratio N_s/N of the design value of surviving number of seg-

ments to the total number of segments that yielded minimum weight was found to be 0.8 or higher. In this study, however, the manifolds were not segmented. Had the manifold been segmented, N_s/N would tend to be lower and conceivably might approach the 0.75 previously reported in the literature.

INTRODUCTION

The heat rejection aspects of electric generating systems for space application have received considerable attention in recent years. It is recognized that a large fraction of the power system weight would be taken up by the waste heat radiator if the conventional fin and tube type were used. Several radiator studies have been reported in the literature for systems up to several megawatts of generated power. A partial list includes references 1 to 6. It would be difficult to relate the results of these studies to one another since each study used different temperature levels, materials, and criteria for calculating protective armor thicknesses.

The analytical study presented herein is an attempt to determine weight trends that might be expected for both segmented and unsegmented direct-condensing fin and tube radiators for a Rankine cycle turboelectric system for the range of power levels from 1 to 10 megawatts electric. No allowance was made for the weight of any necessary radiator support structure. The working fluid was potassium and the materials used were beryllium for the fins and tube armor and columbium for the tube liner. When high and low meteoroid flux estimates were used, weights obtained when segmentation of the tube panels was employed were compared to the unsegmented radiator weights. Of interest also, was the optimum ratio of design value of surviving segments to the total number of segments. Reference 7 had determined the optimum ratio of surviving to total number of segments for an armored radiator without fins and manifolds.

The study objective was to glean trends from many detailed radiator designs that could be used to obtain rough estimates of the effect of power level and segmentation on radiator weight without having to make detailed calculations. Therefore, for comparative purposes, identical cycle conditions were maintained throughout the power range considered. → 20

PROCEDURES AND ASSUMPTIONS

The procedure and the equations used are covered in some detail in appendix B. The development of the equations used to calculate such items as fin thickness, fin length, manifold weight and surface area, tube and manifold pressure drops, and fin and tube angle factors are shown in appendixes C to H.

It was assumed that saturated vapor at 1960° F entered the turbine, the turbine efficiency was 0.8, the generator efficiency was 0.9, and a turbine exit and condensing temperature of 1400° F had the corresponding vapor pressure of about 15 psia. The turbine temperature ratio was taken from reference 8 for minimum radiator area for the 1400° F condensing temperature. Selection of cycle temperatures and efficiencies of the turbine and generator dictates the turbine exit quality, fluid mass flow, and radiator heat load. The calculated turbine exit quality was 0.85, the fluid mass flow was 6.88 pounds per second per megawatt electric, and the radiator heat load, including 100° F subcooling, was 1.8817×10^7 Btu's per hour per megawatt electric.

The following is a brief discussion of other assumptions and restrictions that influence the study results.

Materials

The only materials considered were beryllium for the fins and meteoroid protective armor, and a 0.03-inch columbium liner for the fluid passages.

Radiator Panel Configuration

Two configurations were used, both radiating from both sides. One was a two-panel configuration (fig. 1(a)) with a vapor manifold at one end and a liquid manifold at the other end. The other configuration (fig. 1(b)) with four panels had a central vapor manifold and liquid manifolds at the outer extremities. All manifolds were tapered.

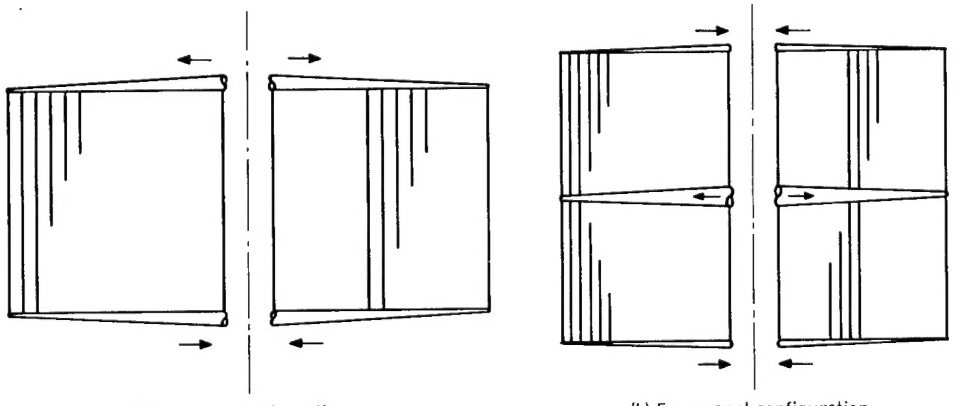

(a) Two-panel configuration. (b) Four-panel configuration.

Figure 1. - Radiator panel arrangement.

Angle Factors

In the radiant heat-transfer treatment, interradiation and interreflection between surfaces were not considered. The angle factors for both the fin and tube took into account only the direct radiation to space. The error introduced by such an assumption has been discussed in reference 9, and the maximum error for the results reported herein was approximately 8 percent. That is, the calculated radiant heat transferred from the fins and tubes was less than the actual amount by a maximum of 8 percent.

Fins and Tubes

Only constant thickness fins and constant diameter tubes were considered even though tapered fins and tubes may have offered some savings in weight. Reference 10 shows a maximum weight savings of 10 percent with tapered fins, but did not include manifold weights. Had the manifold weights been included, the weight savings would have been even less.

Factors Affecting Armor Thickness

Radiator weight is closely tied to the amount of armor necessary to protect against meteoroid damage. The uncertainty of the numbers of particles that would be encountered and of the damage that would be inflicted by any one meteoroid particle makes a calculation of armor thickness somewhat speculative. Several estimates of the meteoroid population are shown graphically in reference 11 and differ by orders of magnitude. The estimates for the density of meteoroids vary from 0.05 to 7.9 grams per cubic centimeter (ref. 12). Due to these wide differences in meteoroid flux and mass estimates, two sets of meteoroid data from reference 11 were used in order to encompass a range. Arbitrarily selected were Whipple's (1961) and Watson's (1956) meteoroid flux estimates. The meteoroid flux and mass estimates and the other important inputs used in the calculation of armor thickness are the following:

(1) Meteoroid flux.

(a) High estimate, Whipple's (1961): $F_{>} = 9.27\times10^{-7}\ m_p^{-10/9}$ particles/$(ft^2)(yr)$ (eq. for curve in ref. 11). The meteoroid density recommended for use with this flux was $\rho_p = 2.7$ grams per cubic centimeter.

(b) Low estimate, Watson's (1956): $F_{>} = 1.19\times10^{-8}\ m_p^{-1}$ particles/$(ft^2)(yr)$ (eq. for curve in ref. 11). A meteoroid density of $\rho_p = 0.5$ gram per cubic centimeter was arbitrarily assumed. The armor thickness is only weakly influenced by particle

density. The meteoroid flux used is the dominant factor in influencing the calculated armor thickness deemed necessary.

(2) Penetration criterion. The model proposed in reference 11 was used. The equation is shown as equation (B7) of appendix B.

(3) Survival probability, 0.9, 0.95, and 0.99.

(4) Mission duration, 2 years.

Manifold Fluid Velocity

Tapered manifolds maintained constant fluid velocities. The fluid velocity was chosen, then the manifold internal diameter was calculated to maintain the velocity picked. For most of the study the fluid velocities used were 200 feet per second in the vapor manifold and 2 feet per second in the liquid. If the sum of the calculated manifold pressure drops exceeded 0.25 psi, the velocities were reduced to 150 feet per second for the vapor and 1 foot per second for the liquid. If the sum of the pressure drops still exceeded 0.25 psi, the vapor velocity was further reduced to 100 feet per second.

Other Assumptions

Radiant input. - The effective sink temperature was assumed to be 0° R.

Working fluid temperature. - The condensing working fluid was assumed to be isothermal everywhere. The fluid stagnation temperature was used to obtain the fluid thermodynamic properties.

Internal tube wall temperature. - The tube internal wall temperature was assumed to be equal to the fluid stagnation temperature.

Subcooling. - The condensed liquid was subcooled 100° F.

Emissivity. - The external radiating surface emissivity was $\epsilon = 0.9$.

PARAMETERS FIXED AS A RESULT OF PRELIMINARY CALCULATIONS

Preliminary calculations were made in an attempt to reduce the number of variables to be used throughout the study. A discussion of these preliminary findings and reasons for picking the values selected follows.

Generalized Length Parameter

In reference 13 the value for the generalized fin length parameter L_g that yielded

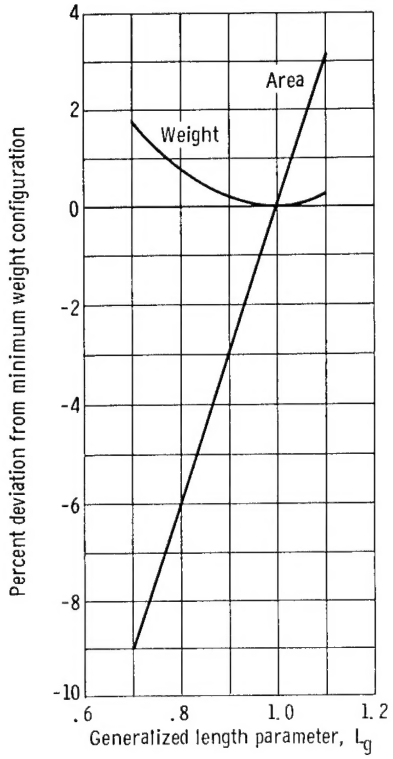

Figure 2. - Effect of generalized length parameter on radiator weight and area. Whipple's flux (1961); system power output, 10 megawatts; probability of receiving no meteoroid puncture during mission duration, 0.9; individual tube length, 40 feet; tube static pressure drop, 1 psi; two-panel configuration.

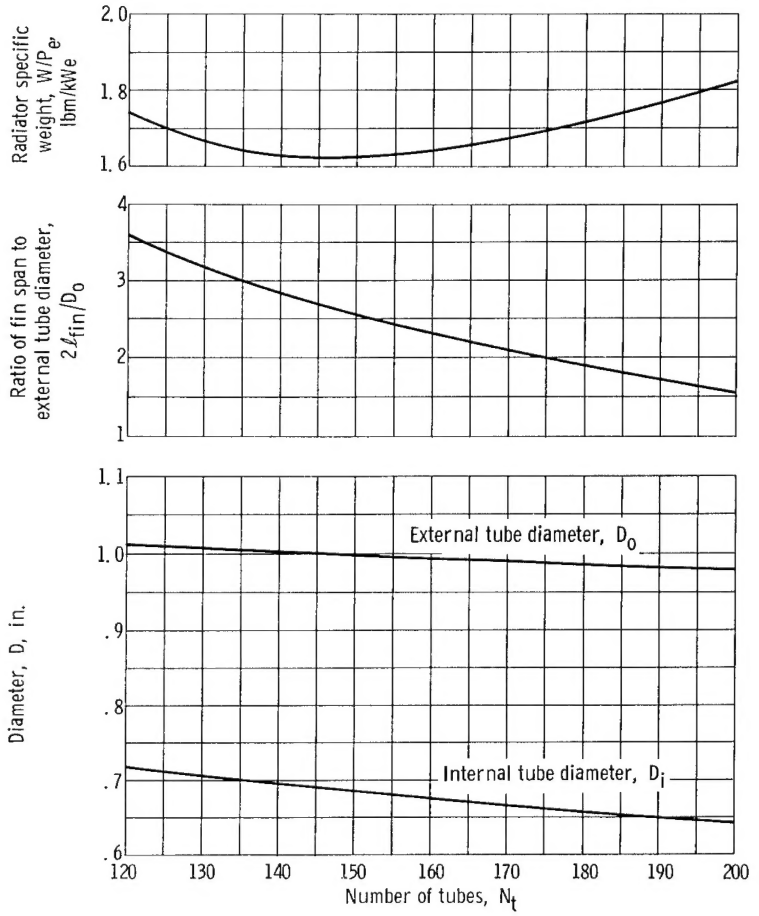

Figure 3. - Specific weight and ratio of fin span to tube outside diameter as function of number of tubes. Watson's flux (1956); system power output, 1 megawatt electric; probability of receiving no meteoroid puncture during mission duration, 0.9; individual tube length, 15 feet; tube static pressure drop, 1 psi; generalized length parameter, 1; two-panel configuration.

the minimum volume fin was approximately 0.92 for the case where the sink temperature was 0° R. The value of L_g that would yield the lightest weight radiator when tubes and manifolds were included was not obvious. Values for L_g of 0.7, 0.92, 1.0, and 1.1 were used to make some preliminary radiator weight and area calculations. For each value of L_g the number of tubes was varied until a minimized weight and corresponding tube diameter were obtained, while everything else such as individual tube length, radiator heat load, and tube pressure drop were held constant. Figure 2 is typical of the result of plotting the percent deviation from minimum weight against L_g. For these preliminary calculations, the minimum weight usually occurred at a value of L_g close to unity. Figures 11 and 12 of reference 10 showed combined fin and tube heat rejection per unit weight, plotted against the ratio of half fin length to tube outer radius, to be maximum for a conductance parameter of about 1. The conductance parameter of reference 10 is identical to L_g^2/ϵ. Using an emissivity ϵ of 0.9 the conductance parameter

of unity (of ref. 10) corresponds to a value for L_g of about 0.95. In reference 10, the particular value of $\ell_{fin}/(D_o/2)$ at which the maximum heat rejection occurred was different for each case shown.

While the approach taken in the study reported herein was somewhat different from that of reference 10, changing the number of fixed length tubes, while maintaining a constant L_g, changes the percentages of the total heat load rejected by the tubes and by the fins. This in essence is the same as changing the ratio $2\ell_{fin}/D_o$. This can be seen from figure 3 where specific weight and $2\ell_{fin}/D_o$ are plotted, for one example, against the number of fixed length tubes. Decreasing N_t increases D_i and D_o but $2\ell_{fin}/D_o$ also increases. Thus for finding minimum radiator weight (constant L_g), changing N_t is equivalent to changing $2\ell_{fin}/D_o$. All of the subsequent radiator weights were obtained by using a value of $L_g = 1$. While a value close to unity provided the minimum weight, it should not be overlooked that by using a lower value of L_g the projected radiator area may be decreased somewhat for only a slight radiator weight penalty. For example, returning to figure 2, when a value of $L_g = 0.7$ is used, the area could be reduced by perhaps 9 percent with a weight increase of about 2 percent. For some applications it might be desirable to accept the higher weight to get the smaller area.

Pressure Drop

The pressure drop across the radiator affects its weight in two ways. The size of the fluid passages is a function of the pressure drop, a high pressure drop permitting small passages. High pressure drop, however, reduces the average condensing temperature as well as adversely affecting the weight of the whole power system by depressing the cycle efficiency; this effect has been ignored in this analysis. Furthermore, a high radiator pressure drop results in a low condensate pump inlet pressure which may make necessary additional subcooling to prevent pump cavitation problems. Figure 4 shows a weight proportionality factor, derived by dividing radiator weight by the weight of an arbitrarily chosen radiator, for three tube pressure drops plotted against the number of tubes for one power level as an illustrative example. The minimum weights for each tube length were about the same for the 1- and 2-psi tube static pressure drops and higher for the 5-psi pressure drop. From figure 4 a tube static pressure drop of 1 psi was chosen for the remainder of the study. This may not be the optimum pressure drop, but the trends being sought should not be influenced significantly. Another 0.25 psi maximum was allowed for the sum of the pressure drops in the vapor and liquid manifold.

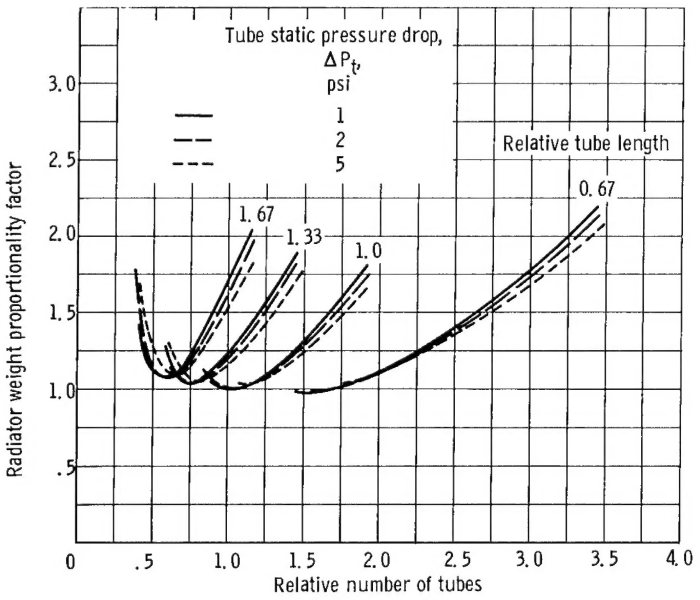

Figure 4. - Effect of pressure drop, tube length, and number of tubes on weight. Meteoroid flux, system power output, probability of receiving meteoroid puncture during mission duration, generalized length parameter, and number of panels are constant.

DISCUSSION OF RESULTS

Radiator calculations were made at four power levels: 1, 2, 5, and 10 megawatts electric. For each power level several tube lengths were considered, and for each tube length specific radiator weight was plotted against the number of tubes. This was done for the unsegmented radiator for all combinations of the three design survival probabilities, two meteoroid flux estimates, and the two panel configurations considered. These plots are too numerous to include, but figure 5 is included as a representative example. Tube length and the number of tubes were varied until the combination that yielded minimum weight was obtained for each power level. In some instances the minimum weight for a particular tube length could not be obtained because the calculations were stopped when the fluid velocity at the tube inlet reached 1300 feet per second. Reference 14 indicates that the vapor velocity for critical two-phase flow (steam water mixtures) is lower than the sonic velocity for the vapor. The equilibrium sonic velocity for potassium saturated vapor (ref. 15) for the 1400° F condensing temperature is about 1450 feet per second. The 1300 feet per second limit was chosen arbitrarily to stay below the vapor equilibrium sonic velocity by a safe margin.

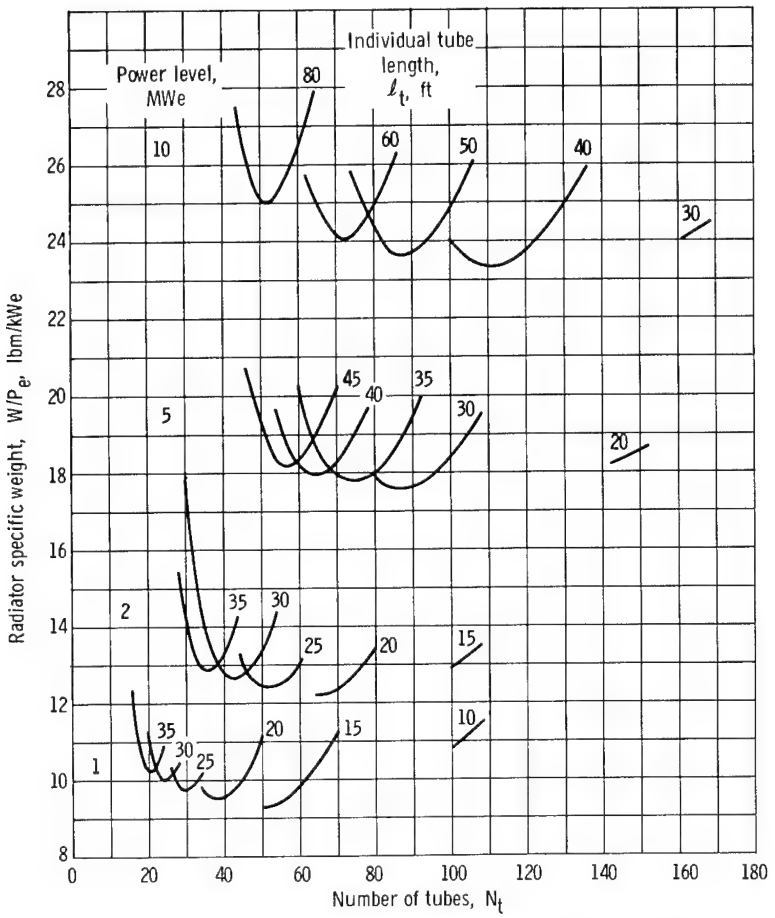

Figure 5. - Effect of tube length and number of tubes on radiator specific weight. Whipple's flux (1961); unsegmented; probability of receiving no meteoroid puncture during mission duration, 0.95; tube static pressure drop, 1 psi; generalized length parameter, 1.0; two-panel configuration.

Effect of Number of Tubes and Tube Length on Tube Internal Diameter

The internal diameter of the tube for any particular radiator may be of interest because of its influence on the area vulnerable to meteoroid puncture as well as heat-transfer considerations. As previously mentioned, a constant tube static pressure drop of 1±0.05 psi was used for the entire study. The internal tube diameter and approximate fluid velocity at tube inlet for any radiator shown in figure 5 can be obtained from figure 6 (p. 10). It is seen from figure 5 that for any given power level increasing the tube length decreases the number of tubes at which the minimum weight occurs and that individual internal tube diameter increases (see fig. 6). Figure 6 also shows that for a given tube length the internal tube diameter is relatively insensitive to changes in the number of tubes, even though the fluid velocity at tube inlet varies considerably. This

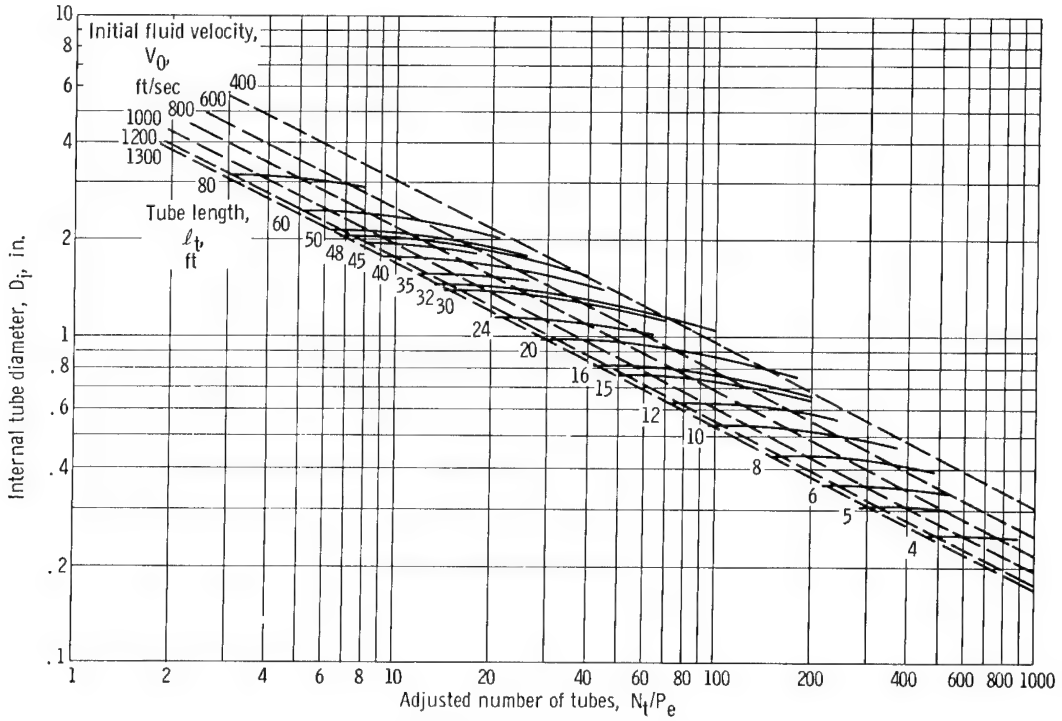

Figure 6. - Internal tube diameter as function of tube length and number of tubes. Tube static pressure drop, 1 psi.

indicates that as inlet velocity increases, increases in friction pressure drop are offset by increases in the momentum pressure rise.

Planform Geometry

The ratio of the width of the radiator to the length in the vehicle axial direction may be important from a vehicle integration standpoint. Flexibility in choosing either dimension without having to pay a severe weight penalty would be desirable. Plots of specific weight against the ratio of total width to radiator length (fig. 7) indicate that some latitude in the choice of planform layout does exist. The minimum weight points from plots similar to figure 5 were plotted to show specific weight as a function of the ratio of radiator width to length in figure 7. Each curve represents the locus of the minimum weight points.

For some of the curves the specific weight was not very sensitive to the width to length ratio. To cite one example, in figure 7(a) for the four-panel configuration for 2 megawatts electric and 0.9 design survival probability using Whipple's (1961) meteoroid flux estimate, the width to length ratio ranged from 0.4 to 10 with a specific weight variation of only about 10 percent. Generally it can be said that as the survival probability is increased or the meteoroid flux estimate is increased, increasing the meteoroid

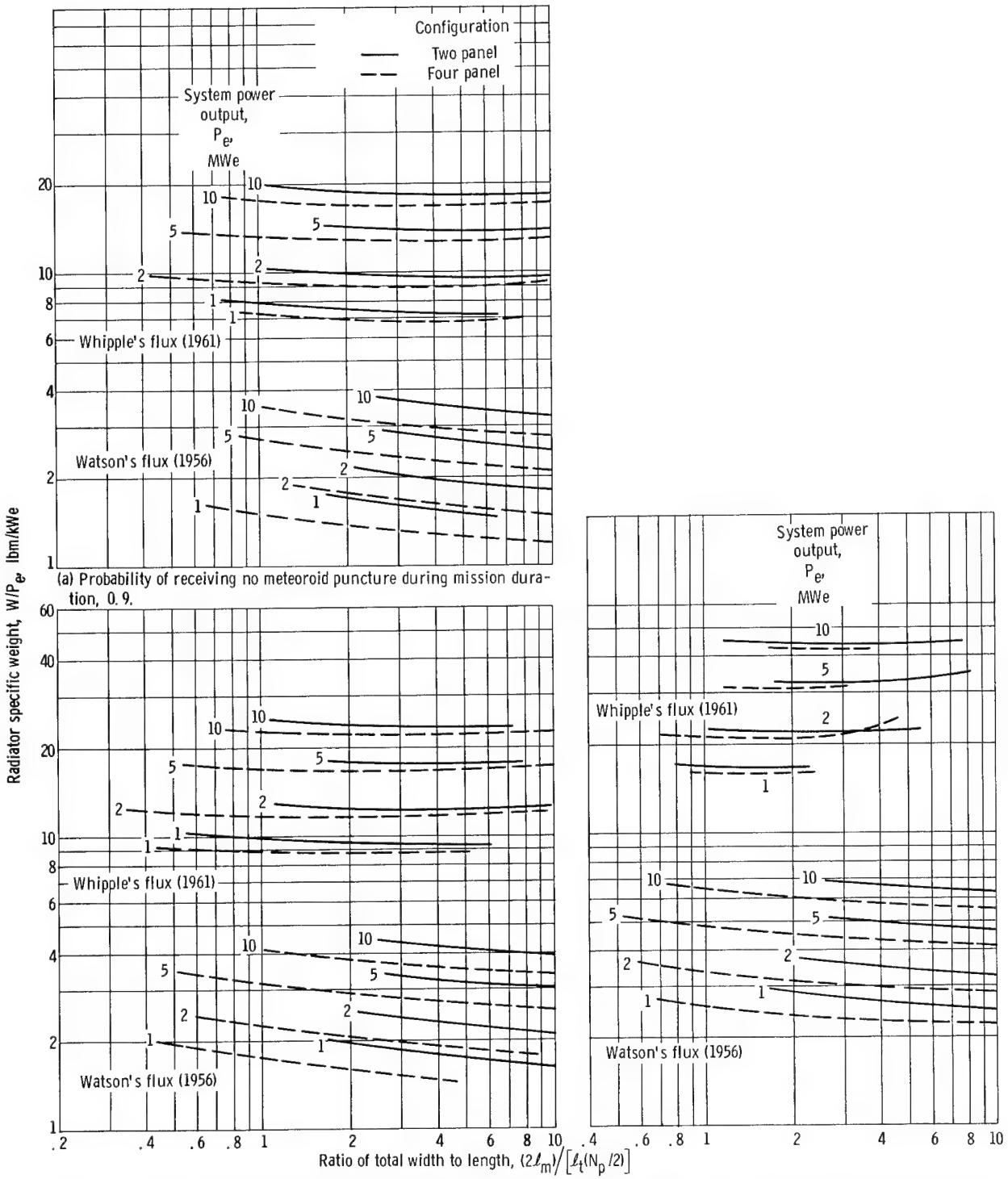

(a) Probability of receiving no meteoroid puncture during mission duration, 0.9.

(b) Probability of receiving no meteoroid puncture during mission duration, 0.95.

(c) Probability of receiving no meteoroid puncture during mission duration, 0.99.

Figure 7. - Effect of ratio of total width to length on radiator specific weight.

protection problem, sensitivity to changes in width to length ratio decreases and the minimum weight panel tends to approach a square.

Influence of Power on Weight

The minimum weights for each combination of power level, survival probability, meteoroid flux, and number of panels were taken from plots similar to figure 5 (p. 9) and used as the basis of the discussion in the section that follows.

When the minimum radiator weights at each of the four system power levels were plotted against the system electrical power, the points on a log-log plot fell in a straight line, which suggested an expression of the form

$$W \propto P_e^b \tag{1}$$

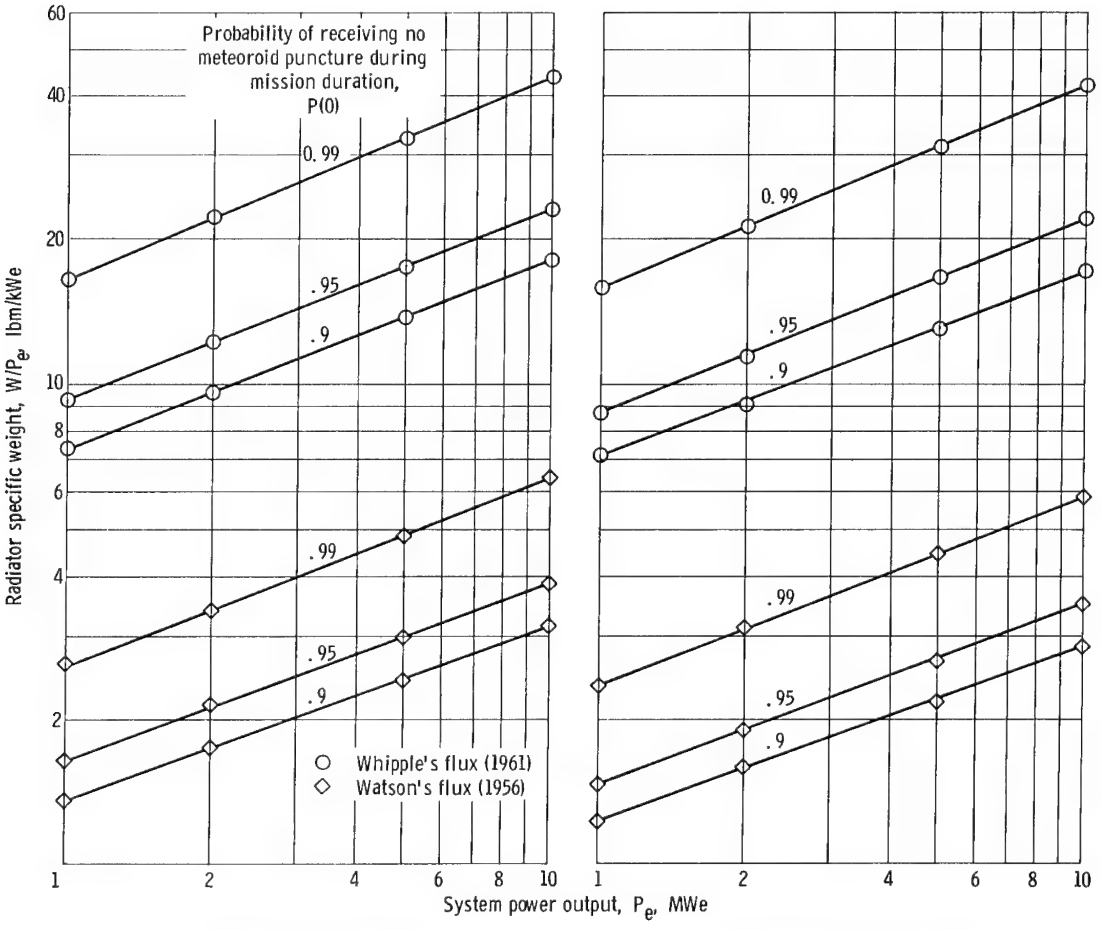

(a) Two-panel configuration.

(b) Four-panel configuration.

Figure 8. - Effect of meteoroid flux estimate, survival probability, and system power level on radiator specific weight.

as used in reference 5. (All symbols are defined in appendix A.) If the value of the constant exponent b is known, radiator weights can be scaled from one power level to another with some degree of confidence.

Equation (1) was rearranged to

$$\frac{W}{P_e} \propto P_e^{b-1} \tag{2}$$

which is the form of the curves plotted in figure 8 for the unsegmented radiator. The use of Whipple's (1961) meteoroid flux estimate, for the 0.9 radiator survival probability, yields radiator specific weights of 7 pounds per kilowatt electric for a 1-megawatt system up to 18 pounds per kilowatt electric for a 10-megawatt system. For the 0.9 survival probability, using Watson's (1956) meteoroid flux estimate, the radiator specific weight ranges from about 1.3 pounds mass per kilowatt electric for a 1-megawatt system to about 3 pounds mass per kilowatt electric for a 10-megawatt system. For the higher 0.99 survival probability, the specific weights were heavier than the specific weights associated with the 0.9 survival probability by a factor of two or more.

The value of b in equation (2) was approximately 1.4 when Whipple's (1961) meteoroid flux estimate was used, and only slightly less when Watson's (1956) meteoroid flux estimate was used. Increasing the design survival probability from 0.9 to 0.99 increased the value of the exponent b only about 2 percent. Also, the value of b was essentially the same for both the two- and four-panel configurations. The value of the exponent reported in reference 5 was 1.5 for a beryllium radiator for a heat load between 1 and 10 megawatts thermal. Results plotted in reference 6 would lead to a value of less than 1.2 for a direct condensing radiator and slightly higher for a liquid filled radiator, both using copper as the fin material.

Segmenting

Reference 7 indicates that segmenting the radiator to reduce the amount of necessary protective armor should offer significant weight savings. Affecting the amount of protective armor necessary for a given overall survival probability are the number of segments N and the design value for the number of segments N_s remaining unpunctured at the end of the mission. Probabilities S of 0.9, 0.95, and 0.99 that at least N_s out of N segments would not be punctured for the 2-year mission duration were assumed to calculate the armor thickness for varying N_s while N was held constant at 10, 20, and finally 100 segments. It should be pointed out that the manifolds were not segmented, only the tube banks, and that calculations were made for the two-panel configuration only.

The equation for calculating the armor thickness is shown in appendix B. Furthermore, it was stipulated that all of the radiator heat load was to be rejected from N_s segments and the manifolds.

Reference 7 showed a figure of merit, which is proportional to weight, plotted as a function of the ratio of N_s to N from which it was concluded that to obtain minimum radiator weight the optimum ratio of N_s to N was approximately 3/4. Reference 7 did not include manifolds and fins. An attempt was made to compare some of the results of reference 7 with the results of this study which does include manifolds and fins.

In reference 7 it was assumed that the required armor thickness t_a was proportional to the cube root of meteoroid particle mass m_p, which in turn was inversely proportional to the meteoroid flux $F_>$:

$$t_a \propto m_p^{1/3} \propto F_>^{-1/3} \tag{3}$$

The $F_>$ is the meteoroid flux having mass m_p or greater. The armor thickness t_a is calculated such that particles smaller than m_p will not penetrate. Therefore, $F_>$ is also the average puncture rate per unit of vulnerable area. Use of the general case where

$$F_> \propto m_p^{-\beta} \tag{4}$$

would have led to

$$t_a \propto m_p^{1/3} \propto F_>^{-1/3\beta} \tag{5}$$

Thus reference 7 has used the special case where $\beta = 1$. For use where $\beta \neq 1$, the equations in reference 7 were rewritten to include β. The figure of merit η is then defined as

$$\eta \equiv \frac{N}{N_s}\left[N_s \ln\left(\frac{1}{p}\right)\right]^{-1/3\beta} \tag{6}$$

The relation between weight and η then becomes

$$\frac{W_s'}{N_s a_v} \propto \eta(N_s a_v \tau)^{1/3\beta} \tag{7}$$

where W'_s is the weight of the segmented prime surface radiator. Reference 7 suggests that for analysis of a given vehicle and mission $N_s a_v \tau$ may be considered to be constant, which makes η a very useful figure of merit in that it is directly proportional to weight. Carrying this further, the ratio of segmented to unsegmented weight can be obtained by

$$\frac{W'_s}{W'_u} = \frac{\eta}{\eta_u} \tag{8}$$

where η_u is the value obtained from equation (6) when the radiator is unsegmented, so that N and N_s are both unity. The values for η presented in reference 7 were for the special case where $\beta = 1$ and this is the value of the exponent used in Watson's (1956) meteoroid flux estimate. Whipple's (1961) meteoroid flux estimate has a value of $\beta = 10/9$, therefore η was recalculated using the new value of β; the W'_s/W'_u was also calculated.

The ratio of segmented to unsegmented weight W_s/W_u, which includes fins and unsegmented manifolds obtained by actually calculating the radiator weights for the segmented and unsegmented radiator is plotted in figure 9 (p. 16) for the high flux estimate and in figure 10 (p. 17) for the low flux estimate. Also plotted in figures 9 and 10 is the ratio W'_s/W'_u, for the prime surface radiator, obtained from equation (8). Just as the survival probability $P(0)$ of the unsegmented radiator was set at 0.9, 0.95, and then 0.99, the overall probability S that N_s out of N segments as well as the manifolds would not be punctured was set at 0.9, 0.95, and then 0.99. Expressed mathmatically for N identical and independent segments,

$$S = P(0)_m \times P(0)_{N_s} = P(0)_m \times \sum_{n=N_s}^{N} \frac{N!}{n!\,(N - n)!}\, p^n (1 - p)^{N-n} \tag{9}$$

The probability that the manifold would not be punctured $P(0)_m$ and the probability that N_s of N segments would remain unpunctured $P(0)_{N_s}$ were equally weighted. With S assigned, $P(0)_m$ and $P(0)_{N_s}$ are simply the square root of S. The individual segment probability of nonpuncture p, which when used in equation (9) yielded the desired value of S, was used when calculating tube armor thickness.

Two generalizations can be made about all of the plots in figures 9 and 10. First, the ratio N_s/N at which the minimum weight occurs is somewhat higher than the expected 0.75 from reference 7. When using Whipple's (1961) meteoroid flux estimate, the

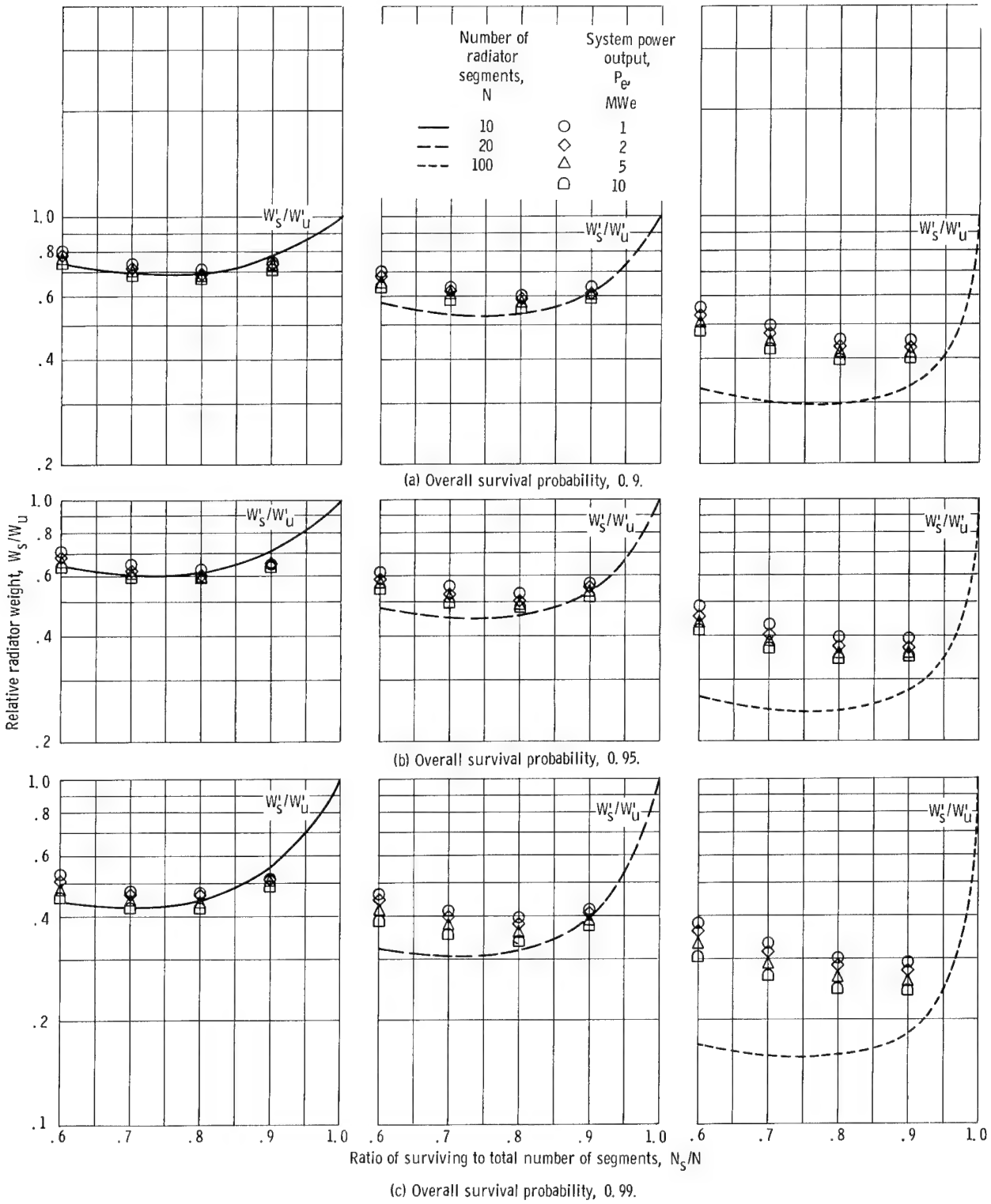

Figure 9. - Effect of number of segments surviving and total number of segments on segmented radiator relative weight. Whipple's flux (1961).

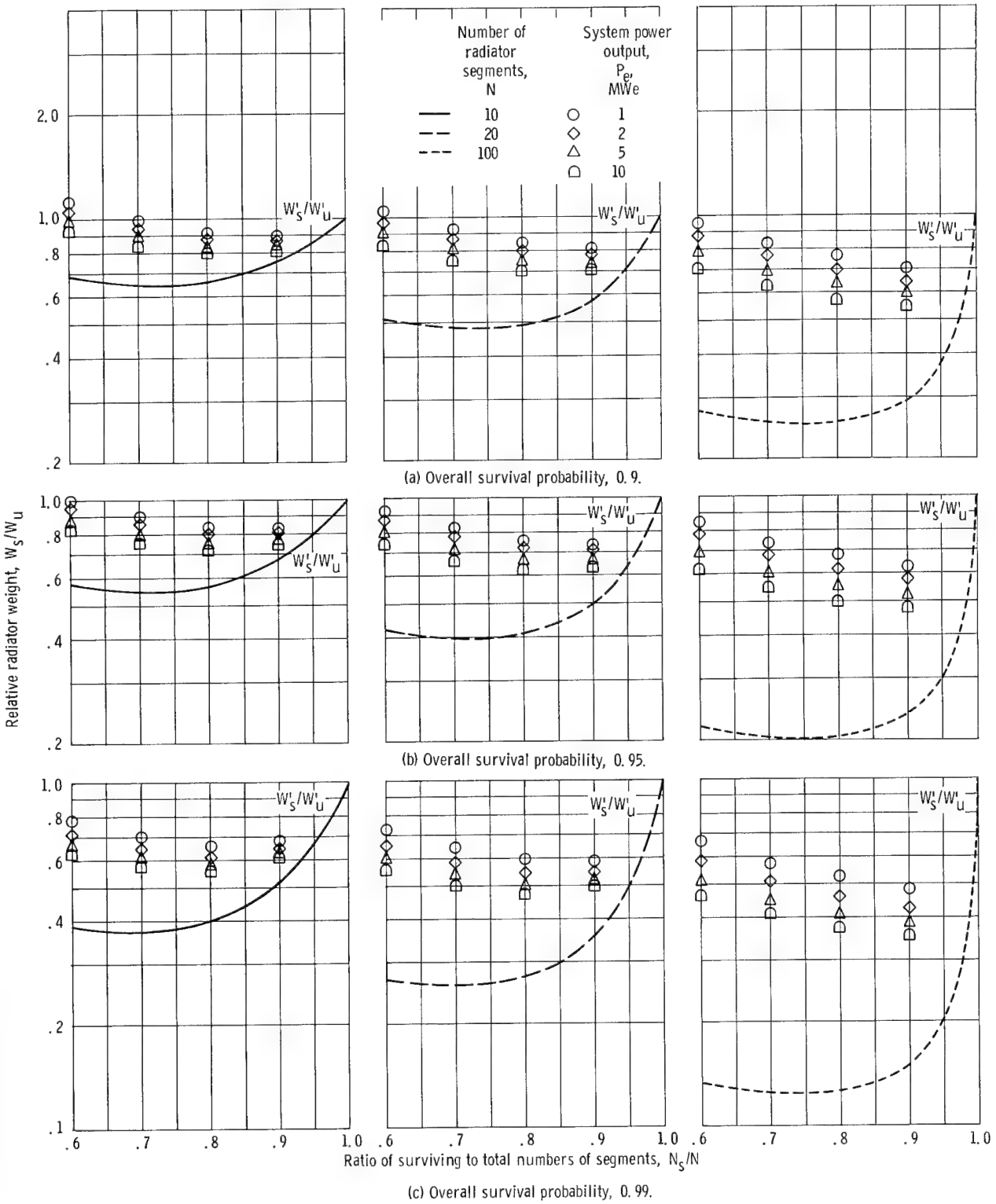

(a) Overall survival probability, 0.9.

(b) Overall survival probability, 0.95.

(c) Overall survival probability, 0.99.

Figure 10. - Effect of number of segments surviving and total number of segments on segmented radiator relative weight. Watson's flux (1956).

minimum weight occurred at N_s/N of 0.8 or higher, and when using Watson's (1956) meteoroid flux estimate, the minimum occurred at N_s/N closer to 0.9. This shift to higher values is probably due to the fact that the manifolds were not segmented. The initial assumption that the entire heat load be rejected from N_s segments means that $N - N_s$ segments are redundant at the start of the mission. Increasing the ratio N_s/N from 0.75 to 0.8 or 0.9 reduces the number of redundant segments, which consequently reduces manifold length and weight.

The second generalization that can be made is that for any given survival probability, number of segments, N_s/N ratio, and meteoroid flux estimate the value of W_s/W_u decreases as the system power level increases; that is, segmenting is more advantageous at higher power levels.

When figure 9 and Whipple's (1961) flux estimate are used, it can be seen that the plot of W'_s/W'_u is a good indicator of the relative weight for 10 and 20 segments, but for 100 segments the level of W_s/W_u is higher than W'_s/W'_u. The curve for W'_s/W'_u applies to a radiator where 100 percent of the weight is protective armor. When Whipple's (1961) meteoroid flux estimate is used for the radiator with fins and unsegmented manifolds, the tube armor comprises only about 60 percent of the total radiator weight. As the number of segments is increased, the tube armor comprises a smaller percentage of the total weight, which makes W'_s/W'_u less applicable as a weight trend indicator. When Watson's (1956) meteoroid flux estimate is used (which is considerably lower than Whipple's, 1961), the tube armor comprises a lesser percentage of the total weight of the radiator with fins and unsegmented manifolds. Thus W'_s/W'_u as a weight trend indicator is even less applicable when Watson's (1956) flux estimate is used for the radiator with unsegmented manifolds as can be seen in figure 10.

It is seen by examining figure 9 that the relative weight W_s/W_u for 10, 20, and 100 segments with Whipple's (1961) flux estimate is approximately 0.7, 0.6, and 0.45, respectively, for a design survival probability of 0.9 and an N_s/N ratio of 0.8, is 0.6, 0.5, and 0.4, respectively, for a design survival probability of 0.95, and is 0.45, 0.4, and 0.3, respectively, for a survival probability of 0.99. Though the weight of any necessary segmenting hardware is not included, substantial weight savings should be attainable.

Figure 10 shows the results when Watson's (1956) meteoroid flux estimate was used. For 100 segments, the minimum relative weight W_s/W_u ranged from 0.55 to 0.7 for a design survival probability of 0.9, from 0.48 to 0.62 for a design survival probability of 0.95, and from 0.35 to 0.48 for a survival probability of 0.99. While the weight savings of segmenting are not as pronounced as when using the more severe Whipple's (1961) flux estimate, segmenting potentially can provide significant weight reduction. Again it should be emphasized that the manifolds were not segmented. Had the manifolds been segmented, even lower relative weights would have been obtained.

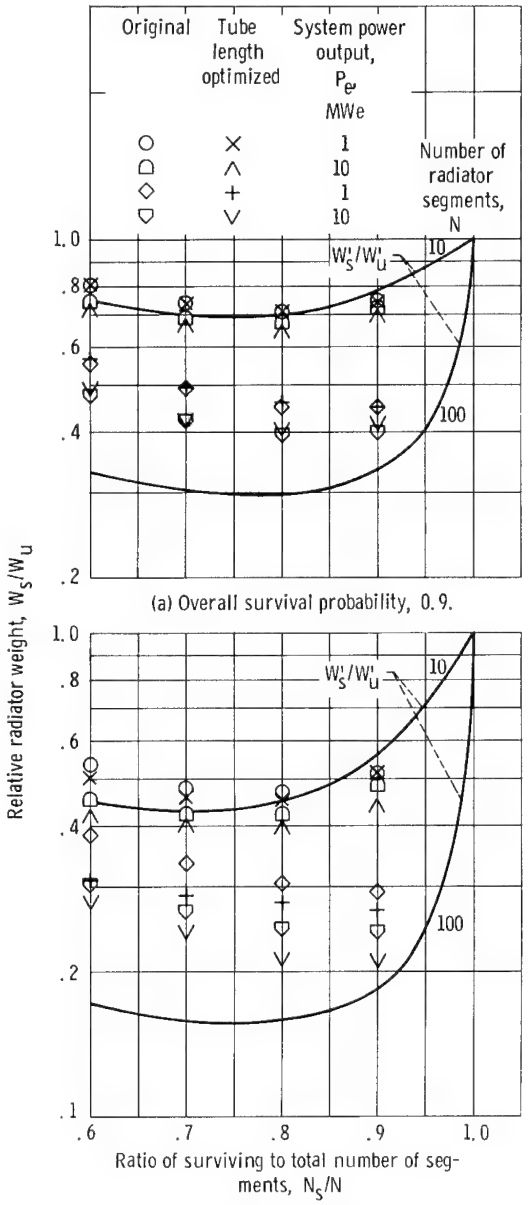

Figure 11. - Relative weight obtained when tube length was optimized, compared to original relative weight. Whipple's flux (1961).

A digression at this point is in order to explain that the segmented radiator was not optimized with respect to the tube length. Even though the tube length associated with the minimum radiator weight, for any given size power system, was not the same for each design survival probability and meteoroid flux, the reference radiator was considered to have tube lengths of 15 feet for the 1-megawatt system, 20 feet for the 2-megawatt system, 30 feet for the 5-megawatt system, and 40 feet for the 10-megawatt system. These lengths were selected from a plot similar to figure 5 (p. 9) but for a design survival probability of 0.9. The same tube lengths were used for all the segmenting calculations. The complete optimization, however, where tube length was also varied was done for comparison by using Whipple's (1961) meteoroid flux for 1- and 10-megawatt-electric power levels and for 10 and 100 segments at each power level. This was done for overall survival probabilities of 0.9 and 0.99. The lightest segmented weight at each N_s/N ratio was used in conjunction with the lightest unsegmented weight. The new values of W_s/W_u were then superimposed on the original plots of figure 9 where S was 0.9 (N = 10, 100) and 0.99 (N = 10, 100), and this is shown in figure 11. The new relative weight was the same as for the nonoptimized plot for S = 0.9 and somewhat lower than the nonoptimized plot for S = 0.99. Thus the relative weights presented in figures 9 and 10 may be somewhat higher than if the tube length had been included in the segmented radiator optimization.

Plotting the minimum weights for segmented tube panels and unsegmented manifolds on a log-log plot against power level (fig. 12, p. 20) resulted in a straight line as it did for the un-

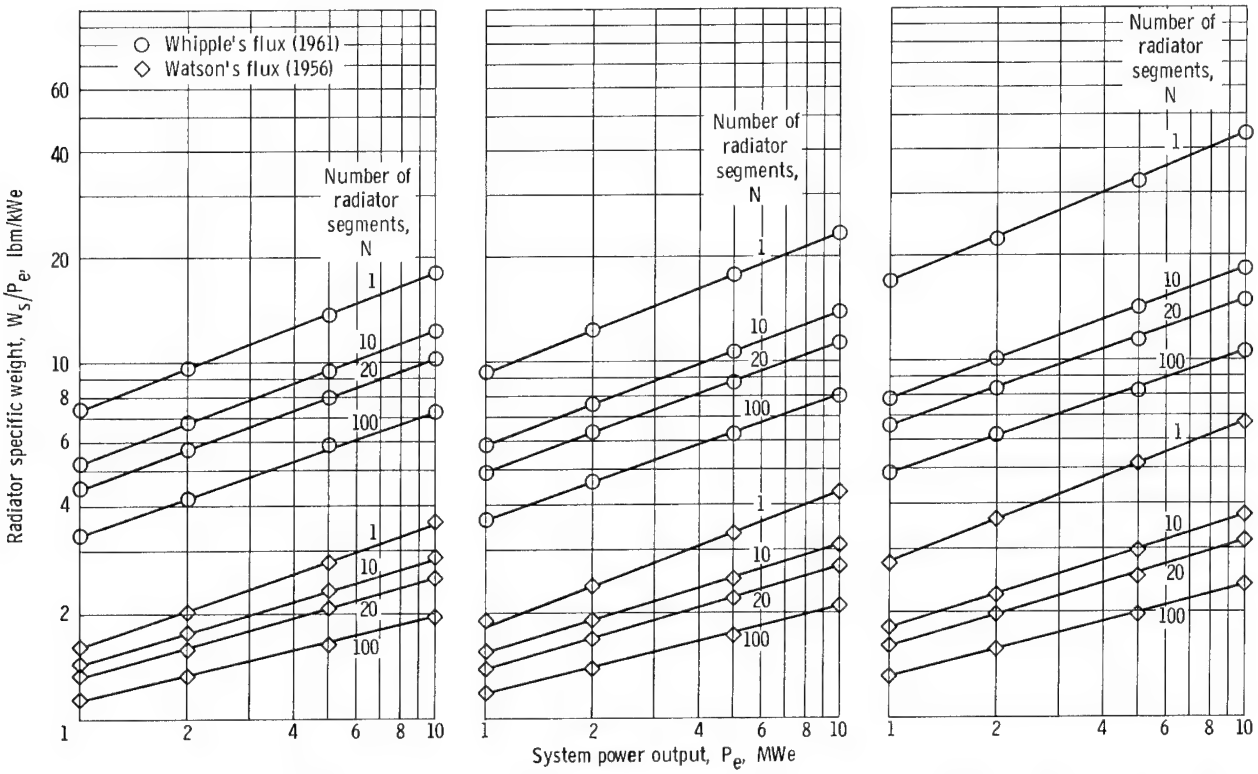

Figure 12. - Effect of meteoroid flux estimate, number of segments, and system power level on segmented radiator specific weight.

segmented case, which again indicated that the weight is proportional to the power level raised to some exponent. For the unsegmented case, the value of the exponent b was about 1.4 and was influenced slightly by the survival probability and the choice of meteoroid flux. When segmenting of the tube panels was employed, b was reduced to lower values. When Whipple's (1961) meteoroid flux estimate was used, the value of b for all three design survival probabilities was 1.37 for 10 segments and 1.34 for 100 segments. With Watson's (1956) meteoroid estimate and the same three design survival probabilities the exponent b was approximately 1.3 for 10 segments and 1.25 for 100 segments. The trends are in the expected direction, because increasing the number of segments or decreasing the severity of the meteoroid flux estimate decreases the amount of necessary protective armor. If no protective armor were necessary, the weight increase with power increase should be almost linear, which means that b would be unity.

CONCLUDING REMARKS

The salient results of the study oriented principally toward radiator weight aspects of large megawatt size Rankine cycle space power systems are as follows:

1. Radiator segmenting can offer significant weight savings especially if high survival probabilities are demanded and/or a high meteoroid flux estimate is used. If a radiator design survival probability of 0.99 were demanded and a severe meteoroid flux such as Whipple's (1961) were used, 100 segments would decrease the weight to less than 0.3 of the weight of an unsegmented radiator. For the same design survival probability and meteoroid flux estimate and as few as 10 segments, the weight of the segmented radiator was still less than half the weight of the unsegmented radiator. With a less severe meteoroid flux estimate such as Watson's (1956), the weight savings, while not as spectacular, are still large enough to make segmentation worthy of consideration. In this study the tube panels were segmented but not the manifolds. If the manifolds had been segmented, the results would differ considerably; undoubtedly greater weight savings would have been possible.

2. The ratio of the design value of surviving segments to total number of segments N_s/N that produced the minimum weight radiator was higher than the expected value of 0.75. Values of 0.8 to 0.9 were found to yield minimum radiator weight, but this upward shift is probably due to the fact that the manifolds were unsegmented. Higher values of N_s/N imply fewer redundant segments, which results in shorter and lighter manifolds. Therefore, if the manifolds had been segmented, the optimum ratio of N_s/N would probably be closer to 0.75.

3. The radiator weight for constant cycle conditions was proportional to the generated power raised to some exponent, $W \propto P_e^b$. The exponent b was a function of the meteoroid flux and the desired survival probability. For the unsegmented beryllium radiator at 1400° F, the value of b was approximately 1.4 when Whipple's (1961) meteoroid flux estimate was used, and just slightly less for Watson's (1956) meteoroid flux estimate. For the segmented radiator, the value of b was lower than for the unsegmented radiator.

Lewis Research Center,
National Aeronautics and Space Administration,
Cleveland, Ohio, October 13, 1965.

APPENDIX A

SYMBOLS

A_m	manifold surface area, ft^2
A_S	surface area, ft^2
A_v	area vulnerable to meteoroid penetration, ft^2
A_w	internal surface area of an individual tube, ft^2
a_s	thin plate and spall adjustment in eq. (B7)
a_v	vulnerable area in one radiator segment in eq. (7), ft^2
b	exponent in eq. (1)
C	defined by eq. (H9)
c	sonic velocity in tube armor, ft/sec
D_i	internal tube diameter, ft
$\mathscr{D}_i$	manifold local internal diameter, ft
D_o	external tube diameter, ft
E_t	Young's modulus, $lbf/in.^2$
e	element of fin
F_{fin}	view factor from fin to space, average
F_t	view factor from tube to space, average
$F_>$	meteoroid flux, particles/(ft^2)(yr)
f	Fanning friction factor
$f(L_g)$	function of generalized length parameter L_g
G	mass velocity, lbm/(ft^2)(sec)
g_c	gravitational constant, 32.2 ft-lbm/(lbf)(sec^2)
h	fluid enthalpy, Btu/lbm
J	Joule's equivalent, 778.2 ft-lbf/Btu
k	thermal conductivity, Btu/(hr)(ft)(^oF)
L_g	generalized length parameter defined by eq. (C2)
ℓ	distance from fin root or distance from manifold entrance, ft
ℓ_{fin}	half fin length, ft
ℓ_m	manifold length, distance along manifold axis between station of maximum diameter and station of minimum diameter, ft
ℓ_t	individual tube length, ft
$\dot{M}$	total fluid mass flow through the radiator, lbm/sec
$\dot{\mathscr{M}}$	local fluid mass flow in individual manifold, lbm/sec
$\dot{m}$	fluid mass flow through individual tube, lbm/sec
m_p	meteoroid particle mass, g
N	number of radiator segments
N_p	number of radiator panels
N_R	Reynolds number

N_s	design value for the number of surviving radiator segments
N_t	number of tubes
n	constant in eq. (B7)
P	static pressure, psi
P_e	system power output, kW or MW
P(0)	probability of receiving no meteoroid puncture during mission duration
p	probability that individual segment will not be punctured by a meteoroid during mission duration
Q_{fin}	heat rejected per unit time from individual fin, Btu/hr
Q_m	heat rejected per unit time from manifolds, Btu/hr
Q_{TOT}	heat rejected from entire radiator, Btu/hr
Q_t	heat extracted from working fluid per unit time per tube, Btu/hr
q_{fin}	heat radiated from individual fin per unit length per unit time, Btu/(hr)(ft)
q_t	heat radiated from tube external surface per unit time per tube, Btu/hr
R	local radius of manifold, ft
S	probability that N_s segments will not be punctured by meteoroids for mission duration
s	manifold surface arc, eq. (F1), ft
T_ℓ	temperature at midfin, ^oR
T_o	fin root temperature, ^oR
T_w	tube internal wall temperature, ^oR
T_x	tube surface temperature, ^oR
ΔT_{sc}	amount of subcooling of the condensate at exit, ^oR
t_a	armor thickness, ft
t_a^*	difference between manifold external and internal radius, ft
t_{fin}	fin thickness, ft
V	fluid velocity, ft/sec
$\mathscr{V}$	material volume, eq. (G3), ft^3
v	fluid specific volume, ft^3/lbm
$\bar{v}$	assumed average meteoroid velocity, ft/sec
W	unsegmented radiator weight, lbm
W_a	tube armor weight, lbm
W_s	segmented radiator weight, lbm
W_u	unsegmented reference radiator weight, lbm
x	vapor quality
β	exponent of particle mass in eq. (4)
γ	coefficient in eq. (B7)
Δ	increment
ϵ	surface emissivity
η	defined by eq. (6)
η_u	value of η when $N = N_s = 1$
θ	velocity exponent in eq. (B7)
μ	fluid viscosity, lbm/(ft)(sec)

ρ	density, lbm/ft^3
σ	Stefan-Boltzman constant, 0.173×10^{-8} $Btu/(hr)(ft^2)(^oR^4)$
τ	mission duration time, yr
Φ, Φ', Φ''	angles defined in appendix H
φ	density exponent in eq. (B7)
φ_g	Lockhart-Martinelli multiplier, eq. (D4)
χ_{tt}	two-phase flow modulus for turbulent-turbulent case, eq. (D5)
ψ	angle in eq. (H8)
Ω	angle in eq. (H6)

Subscripts:

f	liquid
fg	refers to change by evaporation
g	vapor
ℓ	midfin
M	momentum
m	manifold
n	number of times an iterative operation has been performed
p	meteoroid particle
T	target or protective armor
TPF	two-phase friction
t	tube
0	initial

Superscript:

'	refers to prime surface radiator where entire radiator is at one constant temperature

APPENDIX B

ANALYSIS

The calculations for this analysis were performed with a computer program, but instead of showing all the details of the program, only the basic equations that enable the reader to evaluate the method of analysis will be shown. Initial inputs were the radiator heat load, the fluid total temperature and inlet quality, the individual tube length, the number of panels, the desired tube pressure drop, the physical and thermal properties of materials, the initial number of tubes, and a guess of tube internal diameter.

The description is for the unsegmented radiator. The differences between the equations used for the unsegmented and the segmented radiators where the tube banks were segmented will be indicated at the end of this appendix.

Before listing the equations a brief summary of the approach used may be of assistance. First, the individual tube mass flow or the total flow through the radiator divided by the number of tubes, the individual tube length, and the desired tube pressure drop were used to find the tube internal diameter. Then knowing the total tube wall area vulnerable to meteoroid puncture, based on internal diameter, an armor thickness was calculated. With this first estimate for armor thickness the vulnerable area based on tube outer diameter was used to calculate the second estimate of armor thickness. This step was repeated until the ratio of two successive values was unity plus or minus a 1-percent tolerance.

Next the heat radiated from the tube outer surface q_t was calculated. A surface temperature equal to the internal wall temperature, which was assumed to be the same as the fluid total temperature, was used to obtain a first estimate of the heat radiated from the tubes. With the first estimate of q_t the temperature drop through the armor was calculated. With the new surface temperature q_t was recalculated. This was repeated until the surface temperature and q_t were compatible.

Since q_t and the total heat rejection requirement were known, the heat load that had to be rejected by additional finning was determined. Fin dimensions were then calculated, and with this first estimate of fin length the manifold length and surface area were calculated. The armor thickness was recalculated by using the total tube external surface area plus manifold surface area as the area vulnerable. The manifold heat rejection was calculated, heat radiated from the tubes recalculated, and the new fin heat load used to obtain new fin dimensions. This procedure was repeated until the fin geometry was such that the heat rejected from the tubes, manifolds, and fins to space matched the required radiator heat load. Then radiator weight was calculated. The total number of tubes was changed and the process repeated.

The equations used in the analysis are now given. Mass flow through the individual

tube is

$$\dot{m} = \frac{\dot{M}}{N_t} \tag{B1}$$

where $\dot{M}$ is total radiator mass flow and N_t the number of tubes. Since tube mass flow and tube length were known and a guess for tube internal diameter was made, the tube pressure drop was calculated by using the equations given in appendix D:

$$\Delta P_t = -\Delta P_{TPF} + P_M \tag{B2}$$

which is a sum of the two-phase friction and momentum pressure changes. The ΔP_t was tested to see if

$$(\text{Desired } \Delta P_t - 0.05 \text{ psi}) \leq \Delta P_t \leq (\text{Desired } \Delta P_t + 0.05 \text{ psi}) \tag{B3}$$

If ΔP_t did not fall in the desired range, D_i was reestimated by using

$$(D_i)_n = (D_i)_{n-1} \left[\frac{(\Delta P_t)_{n-1}}{\text{Desired } \Delta P_t} \right]^{0.16} \tag{B4}$$

and then ΔP_t was recalculated. The exponent in (B4) was an arbitrary choice based on some preliminary calculations.

When the conditions of (B3) were satisfied, attention was turned to the calculation of the protective armor thickness required. For the first estimate it was said that the tube outer diameter was equal to the tube internal diameter and that manifold vulnerable area A_m was zero:

$$A_{v,t} = \ell_t \pi D_o N_t \tag{B5}$$

$$A_v = A_{v,t} + A_m \tag{B6}$$

Equation (B7), from reference 11, for the armor thickness required was

$$t_a = \frac{a_s}{2.54\times12}\gamma\left(\frac{6}{\pi}\right)^{1/3}\rho_p^{-1/3}\left(\frac{62.4\rho_p}{\rho_t}\right)^{\varphi}\left(\frac{\overline{v}}{c}\right)^{\theta}\left(\frac{\alpha A_v \tau}{-\ln P(0)}\right)^{1/3\beta}\left(\frac{2}{3n\theta\beta + 2}\right)^{1/3\beta} \tag{B7}$$

where

$$a_s = 1.75 \qquad \theta = \frac{2}{3}$$

$$c = 12\sqrt{\frac{E_t g_c}{\rho_t}} \qquad n = 1$$

$$\overline{v} = 98\ 400\ \text{ft/sec} \qquad \gamma = 2$$

$$\varphi = \frac{1}{2}$$

(The values of these parameters were taken from ref. 11 and used herein.)

The first trial had been based on $D_o = D_i$; therefore, D_o was changed to

$$D_o = D_i + 2t_a \tag{B8}$$

and equation (B7) was used to get a new t_a. This was repeated until

$$(D_o)_{n-1} \leq (D_o)_n \leq (D_o)_{n-1} + \frac{0.001}{12} \tag{B9}$$

The heat radiated from each tube was

$$q_{t,0} = \sigma\epsilon\pi D_o \ell_t F_{t,0} T_x^4 \tag{B10}$$

where $F_{t,0} = 0.75$ and $T_x = T_w$ were used as first estimates. Then the tube surface temperature was calculated in accordance with reference 16.

$$T_x = T_w - \frac{q_t \ln\left(\frac{D_o}{D_i}\right)}{2\pi k} \tag{B11}$$

When the new value for T_x was used, q_t was recalculated by using equation (B10). This process was repeated until

$$0.999 \leq \frac{(q_t)_n}{(q_t)_{n-1}} \leq 1.001 \tag{B12}$$

Then the required fin heat load was calculated by using

$$q_{fin} = \frac{1}{2}\left(\frac{Q_{TOT}}{\ell_t N_t} - \frac{q_t}{\ell_t}\right) \tag{B13}$$

Fin thickness and fin length were then calculated by using equations (B14) and (B15) with a first estimate for F_{fin}:

$$t_{fin} = \frac{\left(\frac{q_{fin}}{F_{fin}}\right)^2}{f(L_g) \times 632.5^2 \sigma k \times 2\epsilon \times 10^9 \left(\frac{T_0}{1000}\right)^5} \tag{B14}$$

$$\ell_{fin} = L_g \left[\frac{kt_{fin}}{2\sigma\epsilon 10^9 \left(\frac{T_0}{1000}\right)^3}\right]^{1/2} \tag{B15}$$

The development of equations (B14) and (B15) is shown in appendix C. With the fin length and D_o known, the fin view factor was calculated as shown in appendix H. Then fin thickness and fin length were recalculated by using the new view factor. This was repeated until

$$0.999 \leq \frac{(t_{fin})_n}{(t_{fin})_{n-1}} \leq 1.001 \tag{B16}$$

Next the manifold surface area developed in appendix F was calculated:

$$A_m = A_{m,g} + A_{m,f} = 4\pi\ell_m \left[\frac{2}{3} \left(\frac{\dot{M}}{2\pi\rho_g V_g} \right)^{1/2} + t_a \right] + 2\pi N_p \ell_m \left[\frac{2}{3} \left(\frac{\dot{M}}{\pi N_p \rho_f V_f} \right)^{1/2} + t_a \right] \quad \text{(B17)}$$

For the unsegmented radiator the manifold vulnerable area was included with the tubing vulnerable area by returning to equation (B6) and recalculating everything through equation (B16). When the armor thickness based on the combined tube and manifold area had converged to within ±0.1 percent of the previous value it was accepted.

The heat rejected from the manifold was calculated next. The view factor was assumed to be 0.85 and for a first estimate used $T_{m,g} = T_w$ and $T_{m,f} = T_w - (\Delta T_{sc})/2$:

$$Q_{m,g} = 0.85\sigma\epsilon A_{m,g} T_{m,g}^4 \quad \text{(B18)}$$

$$Q_{m,f} = 0.85\sigma\epsilon A_{m,f} T_{m,f}^4 \quad \text{(B19)}$$

$$Q_m = Q_{m,g} + Q_{m,f} \quad \text{(B20)}$$

where the subscript g refers to the vapor manifold and f to the liquid manifold. Then the manifold external temperatures were calculated by treating the manifold as a flat plate of area $A_{m,g}$ or $A_{m,f}$ and thickness t_a:

$$T_{m,g} = T_w - \frac{Q_{m,g} t_a}{k A_{m,g}} \quad \text{(B21)}$$

$$T_{m,f} = \left(T_w - \frac{\Delta T_{sc}}{2} \right) - \frac{Q_{m,f} t_a}{k A_{m,f}} \quad \text{(B22)}$$

Then $Q_{m,g}$ and $Q_{m,f}$ were recalculated by using the calculated values for $T_{m,g}$ and $T_{m,f}$. This was repeated until

$$0.999 \leq \frac{(Q_m)_n}{(Q_m)_{n-1}} \leq 1.001 \quad \text{(B23)}$$

The heat to be rejected by the fin was recalculated:

$$q_{fin} = \frac{1}{2}\left[\frac{Q_{TOT} - Q_m - N_t q_t\left(\frac{F_t}{F_{t,0}}\right)}{\ell_t N_t}\right] \tag{B24}$$

The F_t was calculated as shown in appendix H. With the new value for q_{fin} the program returned to equation (B14) to calculate a new t_{fin}. Everything from equation (B14) to (B24) was repeated until

$$0.999 \leq \frac{\left(q_{fin}\right)_n}{\left(q_{fin}\right)_{n-1}} \leq 1.001 \tag{B25}$$

Then the total vulnerable area was calculated and checked against the previous value to see that

$$0.999 \leq \frac{\left(A_v\right)_n}{\left(A_v\right)_{n-1}} \leq 1.001 \tag{B26}$$

If the condition of equation (B26) was not met, the program returned to equation (B6). When the ratio fell within the range specified in equation (B26), the manifold pressure drops and radiator weight were calculated.

The pressure drops in the manifolds were calculated by the equations developed in appendix E. The fluid velocities V_g and V_f were assumed. The actual values used are listed in the assumptions in the text. The working fluid properties were obtained from reference 15:

$$\Delta P_{m,g} = \frac{2\varphi_{g,0}^2 \rho_g V_g^2 \ell_m}{144 g_c \left(\frac{2\dot{M}}{\pi \rho_g V_g}\right)^{1/2}}\left[0.0028 + \frac{0.3676}{\left(\frac{2\dot{M}\rho_g V_g}{\pi \mu_g^2}\right)^{0.16}}\right] \tag{B27}$$

$$\Delta P_{m,f} = \frac{2\rho_f V_f^2 \ell_m}{144 g_c \left(\frac{4\dot{M}}{N_p \pi \rho_f V_f}\right)^{1/2}}\left[0.0028 + \frac{0.3676}{\left(\frac{4\dot{M}\rho_f V_f}{N_p \pi \mu_f^2}\right)^{0.16}}\right] \tag{B28}$$

The manifold weight equations from appendix G were

$$W_{m,g} = 2\rho_T \pi t_a \ell_m \left[\frac{4}{3} \left(\frac{\dot{M}}{2\rho_g \pi V_g} \right)^{1/2} + t_a \right] \tag{B29}$$

$$W_{m,f} = N_p \rho_T \pi t_a \ell_m \left[\frac{4}{3} \left(\frac{\dot{M}}{N_p \rho_f \pi V_f} \right)^{1/2} + t_a \right] \tag{B30}$$

and the remaining weights were

$$W_{fin} = 2\rho_{fin} \ell_t N_t \ell_{fin} t_{fin} \tag{B31}$$

$$W_a = \rho_T \ell_t N_t \frac{\pi}{4} \left(D_o^2 - D_{o,liner}^2 \right) \tag{B32}$$

$$W_{liner} = \rho_{liner} \ell_t N_t \frac{\pi}{4} \left(D_{o,liner}^2 - D_i^2 \right) \tag{B33}$$

$$W = W_{m,g} + W_{m,f} + W_{fin} + W_a + W_{liner} \tag{B34}$$

Modifications for Segmenting

Segmenting was employed to reduce the amount of protective armor necessary to maintain the same radiator survival probability as for the unsegmented radiator. Redundant radiator sections were carried so that if an active radiator section were punctured by a meteoroid the damaged section would be isolated and one of the redundant sections activated. Thus the radiator with N segments was designed to reject the entire heat load from N_s segments, N_s being the design value for the number of segments which would remain unpunctured at the end of the mission. This requires minor modifications of the equations used for the unsegmented radiator. First of all, since only N_s segments out of a total of N segments are active, the number of active tubes is the fraction N_s/N times the total number of tubes. Thus in equations (B1), (B13), and (B24) where N_t appears it is replaced by $N_t(N_s/N)$.

The other, and most important difference, is the procedure for calculating the armor thicknesses. The armor thickness for the manifold was calculated separately from the tube armor thickness. This was necessary because the manifolds were not segmented,

only the tube banks. The overall survival probability S that the manifolds and N_s out of N independent segments would remain unpunctured is

$$S = P(0)_m P(0)_{N_s} = P(0)_m \sum_{n=N_s}^{N} \frac{N!}{(N-n)!n!} p^n (1-p)^{N-n} \tag{B35}$$

The value of S was assigned and $P(0)_m$, the probability that the manifolds would not be punctured, and $P(0)_{N_s}$, the probability that N_s of N segments would remain unpunctured, were weighted equally, or

$$P(0)_m = P(0)_{N_s} = \sqrt{S} \tag{B36}$$

A value of p, the probability that any individual segment would not be punctured, was found so that

$$P(0)_{N_s} = \sum_{n=N_s}^{N} \frac{N!}{(N-n)!n!} p^n (1-p)^{N-n} = \sqrt{S} \tag{B37}$$

The tube vulnerable area of an individual segment is

$$a_v = \frac{A_{v,t}}{N} = \frac{N_t}{N} \ell_t \pi D_o \tag{B38}$$

Then the tube armor thickness would be calculated by using equation (B7) with this modification. The term $\left[\alpha A_v \tau / -\ln P(0)\right]^{1/3\beta}$ was replaced by the term $\left(\alpha a_v \tau / -\ln p\right)^{1/3\beta}$. Similarly the manifold armor thickness was calculated by using equation (B7) with the term $\left[\alpha A_v \tau / -\ln P(0)\right]^{1/3\beta}$ replaced by $\left[\alpha A_m \tau / -\ln P(0)_m\right]^{1/3\beta}$. Equation (B6) is deleted when calculating the segmented radiator. Essentially these were the only important differences between the segmented and unsegmented calculation procedures.

APPENDIX C

FIN LENGTH AND THICKNESS

The equations for calculating half fin length ℓ_{fin} and fin thickness, t_{fin} with fin width ℓ_t held constant were taken from reference 13. One modification, adding a fin view factor, was made to account for the fact that the fin did not have an unrestricted view of space, see sketch (a).

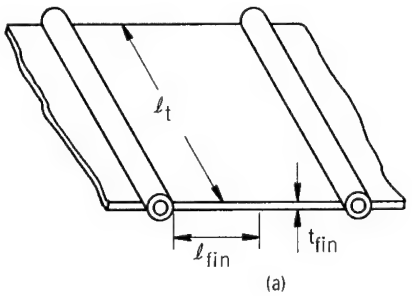

(a)

$$\frac{\ell_{fin} t_{fin} \ell_t}{\frac{Q_{fin}}{F_{fin}}} = \frac{\left(\frac{Q_{fin}}{F_{fin}\ell_t}\right)^2 L_g}{(632.46)^3\left[f(L_g)\right]^{3/2}\sigma^2 10^{18} k(2\epsilon)^2\left(\frac{T_o}{1000}\right)^9} \tag{C1}$$

and

$$L_g = \ell_{fin}\sqrt{\frac{2\sigma\epsilon}{kt_{fin}}\,10^9\left(\frac{T_o}{1000}\right)^3} \tag{C2}$$

Substituting equation (C2) into (C1) and simplifying yield

$$t_{fin} = \frac{\left(\frac{Q_{fin}}{F_{fin}\ell_t}\right)^2}{f(L_g)(632.46)^2\sigma k 2\epsilon 10^9\left(\frac{T_o}{1000}\right)^5} \tag{C3}$$

Since L_g has been chosen and the equivalent sink temperature was assumed to be zero, T_ℓ can be obtained from figure 8 of reference 13. With T_ℓ known and $f(L_g)$ obtained from equation (39) of reference 13, t_{fin} can be found from equation (C3). It remains then to solve for ℓ_{fin} in equation (C2).

APPENDIX D

TWO-PHASE PRESSURE DROP IN A CONSTANT DIAMETER TUBE

The flow regime assumed was that of a homogeneous mixture with both the liquid and vapor traveling at the same velocity. To obtain two-phase pressure drop, the single-phase multiplier of reference 17 was used.

The tube was divided into increments and the two-phase friction static pressure drop for each increment was calculated by using the local vapor velocity. Because the condensing process is essentially isothermal the wall heat flux was deemed to be constant.

The energy equation as applied to the increment is

$$h_n - h_{n-1} + \frac{V_n^2 - V_{n-1}^2}{2g_c J} = \frac{4\dfrac{Q_t}{A_w}\,\Delta\ell_t}{3600\,GD_i} \tag{D1}$$

For the initial calculation the velocity term was neglected but then considered after the local vapor quality

$$x_n = \frac{h_n - h_f}{h_{fg}} \tag{D2}$$

was found. The average quality for the increment is then

$$x_{n,n-1} = \frac{x_{n-1} + x_n}{2} \tag{D3}$$

The use of the average quality will be evident after showing the pressure drop equation. From reference 17

$$\left(\frac{\Delta P}{\Delta\ell_t}\right)_{TPF} = \varphi_g^2\left(\frac{\Delta P}{\Delta\ell_t}\right)_g \tag{D4}$$

where φ_g is a function of χ. For the assumed turbulent-turbulent case,

$$\chi_{tt} = \left(\frac{\rho_g}{\rho_f}\right)^{0.5} \left(\frac{\mu_f}{\mu_g}\right)^{0.1} \left(\frac{\dot{m}_f}{\dot{m}_g}\right)^{0.9} \tag{D5}$$

The fluid density ρ and viscosity μ were evaluated at inlet total temperature and pressure. The weight flow of the liquid $\dot{m}_f$ and the weight flow of the vapor $\dot{m}_g$ can be expressed as a function of the vapor quality

$$\dot{m}_f = (1 - x)\dot{m} \tag{D6}$$

and

$$\dot{m}_g = x\dot{m} \tag{D7}$$

Thus,

$$\left(\chi_{tt}\right)_{n,n-1} = \left(\frac{\rho_g}{\rho_f}\right)^{0.5} \left(\frac{\mu_f}{\mu_g}\right)^{0.1} \left(\frac{1}{x_{n,n-1}} - 1\right)^{0.9} \tag{D8}$$

A curve fit for the plot of φ_g against χ_{tt} was used to obtain φ_g. Then

$$\left(\Delta P_{TPF}\right)_{n,n-1} = \frac{2\rho_g \left(\varphi_g^2 f V_g^2\right)_{n,n-1} \Delta \ell_t}{144 g_c D_i} \tag{D9}$$

where

$$\left(V_g\right)_{n,n-1} = G x_{n,n-1} v_g \tag{D10}$$

and

$$f_{n,n-1} = 0.0014 + \frac{0.125}{\left(\frac{D_i \rho_g \left(V_g\right)_{n,n-1}}{\mu_g}\right)^{0.32}} \tag{D11}$$

Equation (D11) is the empirical relation of Koo (ref. 16) and is valid for the range of N_R from 3 000 to 3 000 000. This was chosen instead of the Blasius friction factor, recommended in reference 17, because it was applicable over a wider range of Reynolds numbers. Then h_n was corrected for the change in velocity across the increment and the pressure drop for the next increment found. The friction two-phase pressure drop was added to the momentum pressure rise:

$$\Delta P_t = -\Delta P_{TPF} + \Delta P_M = -\sum_{n=1}^{\ell_t/\Delta\ell_t} \frac{\left[2(\varphi_g)^2_{n,n-1}\rho_g(V_g)^2_{n,n-1} f_{n,n-1}\,\Delta\ell_t\right]_n}{144\, g_c D_i} + \frac{G^2 x_0 v_{fg}}{144 g_c} \qquad \text{(D12)}$$

APPENDIX E

MANIFOLD PRESSURE DROP

It was approximated that the fluid mass flow in the manifold decreased linearly with manifold length. The mass flow at any station ℓ is then

$$\dot{\mathscr{M}} = \dot{\mathscr{M}}_0 \left(1 - \frac{\ell}{\ell_m}\right) \tag{E1}$$

where $\dot{\mathscr{M}}$ denotes the local fluid mass flow in the individual manifold. For the vapor manifold,

$$\dot{\mathscr{M}}_0 = \frac{\dot{M}}{2}$$

and for the liquid manifold

$$\dot{\mathscr{M}}_0 = \frac{\dot{M}}{N_p}$$

Also

$$\mathscr{D}_i = 2R$$

Secondly, it was stipulated that the manifold diameter would be varied to maintain a constant fluid velocity for the decreasing mass flow.

The two-phase friction pressure drop in the vapor manifold is

$$\left(\frac{dP}{d\ell}\right)_{TPF} = \frac{2\varphi_g^2 f \rho_g V_g^2}{144 g_c \mathscr{D}_i} \tag{E2}$$

When Koo's empirical equation (ref. 16), is used

$$f = 0.0014 + \frac{0.125}{(N_R)^{0.32}} \tag{E3}$$

which is valid for $3\ 000 \leq N_R \leq 3\ 000\ 000$ and

$$N_R = \frac{\mathscr{D}_i V_g \rho_g}{\mu_g} \tag{E4}$$

Substituting equations (E3) and (E4) into (E2) yields

$$\left(\frac{dP}{d\ell}\right)_{TPF} = \frac{2\varphi_g^2 \rho_g V_g^2}{144 g_c \mathscr{D}_i} \left[0.0014 + \frac{0.125}{\left(\frac{V_g \rho_g}{\mu_g}\right)^{0.32} \mathscr{D}_i^{0.32}}\right] \tag{E5}$$

Mass flow is

$$\dot{\mathscr{M}} = \frac{\pi}{4} \mathscr{D}_i^2 \rho_g V_g \tag{E6}$$

Rearranging (E6) and substituting (E1) yield

$$\mathscr{D}_i = \left(\frac{4\dot{\mathscr{M}}}{\pi \rho_g V_g}\right)^{1/2} = \left[\frac{4\dot{\mathscr{M}}_0}{\pi \rho_g V_g}\left(1 - \frac{\ell}{\ell_m}\right)\right]^{1/2} \tag{E7}$$

Substituting equation (E7) into (E5) and assuming that the change in vapor quality is small enabling ρ_g, μ_g, and φ_g in addition to V_g to be treated as constants yield equation (E5) as

$$\int_{\ell=0}^{\ell=\ell_m} dP_{TPF} = \frac{2\varphi_g^2 \rho_g V_g^2}{144 g_c} \left[\frac{0.0014}{\left(\frac{4\dot{\mathscr{M}}_0}{\pi \rho_g V_g}\right)^{1/2}} \int_{\ell=0}^{\ell=\ell_m} \frac{d\ell}{\left(1 - \frac{\ell}{\ell_m}\right)^{1/2}} + \frac{0.125}{\left(\frac{\rho_g V_g}{\mu_g}\right)^{0.32} \left(\frac{4\dot{\mathscr{M}}_0}{\pi \rho_g V_g}\right)^{0.66}} \int_{\ell=0}^{\ell=\ell_m} \frac{d\ell}{\left(1 - \frac{\ell}{\ell_m}\right)^{0.66}}\right] \tag{E8}$$

Integration of equation (E8) for the vapor manifold friction pressure drop and substitution for $\dot{M}_0$ yield

$$\Delta P_{m,g} = \frac{2\varphi_g^2 \rho_g V_g^2 \ell_m}{144 g_c \left(\frac{2\dot{M}}{\pi \rho_g V_g}\right)^{1/2}} \left[0.0028 + \frac{0.3676}{\left(\frac{2\dot{M}\rho_g V_g}{\pi \mu_g^2}\right)^{0.16}}\right] \tag{E9}$$

For the liquid manifold, the friction drop is

$$\Delta P_{m,f} = \frac{2\rho_f V_f^2 \ell_m}{144 g_c \left(\frac{4\dot{M}}{\pi N_p \rho_f V_f}\right)^{1/2}} \left[0.0028 + \frac{0.3676}{\left(\frac{4\dot{M}\rho_f V_f}{N_p \pi \mu_f^2}\right)^{0.16}}\right] \tag{E10}$$

APPENDIX F

MANIFOLD SURFACE AREA

The manifold external surface area must be calculated and included as part of the area vulnerable to meteoroid puncture. Also, it is required to calculate the quantity of heat radiated to space directly from the manifold.

Using the notation shown in sketch (b) the external surface area is

$$A_S = \int_0^s 2\pi \left(R + t_a^*\right) ds \approx \int_0^s 2\pi (R + t_a) ds \tag{F1}$$

$$ds = \sqrt{1 + \left(\frac{dR}{d\ell}\right)^2}\, d\ell \tag{F2}$$

In equation (E7) it was shown that

$$R = \left[\frac{\dot{\mathcal{M}}_0}{\pi \rho V}\left(1 - \frac{\ell}{\ell_m}\right)\right]^{1/2}$$

Then

$$\frac{dR}{d\ell} = \frac{1}{2}\left(\frac{\dot{\mathcal{M}}_0}{\pi \rho V}\right)^{1/2}\left(-\frac{1}{\ell_m}\right)\left(1 - \frac{\ell}{\ell_m}\right)^{-1/2} \tag{F3}$$

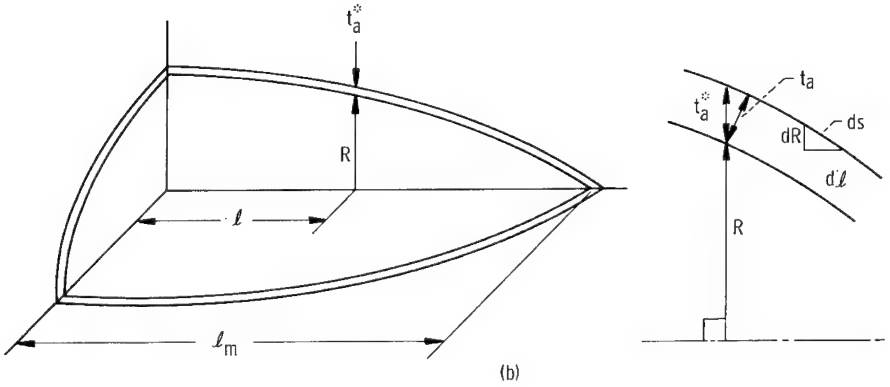

(b)

and

$$\left(\frac{dR}{d\ell}\right)^2 = \frac{\dot{\mathscr{M}}_0}{4\pi\rho V \ell_m^2}\left(1 - \frac{\ell}{\ell_m}\right)^{-1} \tag{F4}$$

Substituting equations (F2) and (F4) yields equation (F1) as

$$A_S = 2\pi\left\{\int_{\ell=0}^{\ell_m}\left[\frac{\dot{\mathscr{M}}_0}{\pi\rho V}\left(1 - \frac{\ell}{\ell_m}\right)\right]^{1/2}\left[1 + \frac{\dot{\mathscr{M}}_0}{4\pi\rho V\ell_m^2}\frac{1}{\left(1 - \frac{\ell}{\ell_m}\right)}\right]^{1/2} d\ell + t_a\int_{\ell=0}^{\ell_m}\left[1 + \frac{\dot{\mathscr{M}}_0}{4\pi\rho V\ell_m^2}\frac{1}{\left(1 - \frac{\ell}{\ell_m}\right)}\right]^{1/2} d\ell\right\} \tag{F5}$$

Integration of equation (F5) yields

$$A_S = 2\pi\left\{\frac{1}{12\ell_m^2}\left[\left(4\ell_m^2 + \frac{\dot{\mathscr{M}}_0}{\pi\rho V}\right)^{3/2}\left(\frac{\dot{\mathscr{M}}_0}{\pi\rho V}\right)^{1/2} - \left(\frac{\dot{\mathscr{M}}_0}{\pi\rho V}\right)^2\right] + t_a\left[\left(\ell_m^2 + \frac{\dot{\mathscr{M}}_0}{4\pi\rho V}\right)^{1/2} \pm \frac{\dot{\mathscr{M}}_0}{4\pi\rho V\ell_m}\tanh^{-1}\left(\frac{1}{1 + \frac{\dot{\mathscr{M}}_0}{4\pi\rho V\ell_m^2}}\right)^{1/2}\right]\right\} \tag{F6}$$

This cumbersome expression was simplified after closer examination. First, $\ell_m > 1$, therefore $\ell_m^2 >> 1$ and it was found that $\dot{\mathscr{M}}_0/\rho\pi V << 1$; therefore, $\ell_m^2 >> \dot{\mathscr{M}}_0/4\rho\pi V$. The troublesome term in equation (F6) was the inverse hyperbolic tangent. As

$$\left(\frac{\dot{\mathscr{M}}_0}{4\pi\rho V\ell_m^2}\right) \to 0$$

the

$$\tanh^{-1}\left(\frac{1}{1+\frac{\dot{M}_0}{4\pi\rho V\ell_m^2}}\right)\to\infty$$

However, looking at the expression practically, if

$$\frac{\dot{M}_0}{4\pi\rho V\ell_m^2} > 2\times10^{-5}$$

then

$$\tanh^{-1}\left(\frac{1}{1+\frac{\dot{M}_0}{4\pi\rho V\ell_m^2}}\right) < 5.7$$

To simplify then, the insignificant terms in equation (F6) were deleted yielding

$$A_S \cong 2\pi\left\{\left[\frac{\left(4\ell_m^2\right)^{3/2}}{12\ell_m^2}\right]\left(\frac{\dot{M}_0}{\pi\rho V}\right)^{1/2} + t_a\left(\ell_m^2\right)^{1/2}\right\} \tag{F7}$$

or

$$A_S \cong 2\pi\ell_m\left[\frac{2}{3}\left(\frac{\dot{M}_0}{\pi\rho V}\right)^{1/2} + t_a\right] \tag{F8}$$

The manifold surface areas then are

$$A_{m,g} = 4\pi\ell_m\left[\frac{2}{3}\left(\frac{\dot{M}}{2\pi\rho_g V_g}\right)^{1/2} + t_a\right] \tag{F9}$$

$$A_{m,f} = 2N_p \pi \ell_m \left[\frac{2}{3} \left(\frac{\dot{M}}{N_p \pi \rho_f V_f} \right)^{1/2} + t_a \right] \tag{F10}$$

$$A_m = A_{m,g} + A_{m,f} \tag{F11}$$

APPENDIX G

MANIFOLD WEIGHT

As in appendix E this is the development of the general case for the individual manifold using $\dot{\mathscr{M}}$ to denote local fluid mass flow in the individual manifold. The sketch in appendix F is also applicable here.

The volume of material is

$$\mathscr{V} \cong \int_0^{\ell_m} \left[\pi\left(R + t_a\right)^2 - \pi R^2\right] d\ell \tag{G1}$$

assuming $t_a^* \cong t_a$. Simplifying and substituting equation (E7) into (G1) yield

$$\mathscr{V} \cong \pi\left[2t_a\left(\frac{\dot{\mathscr{M}}_0}{\rho\pi V}\right)^{1/2}\int_{\ell=0}^{\ell_m}\left(1 - \frac{\ell}{\ell_m}\right)^{1/2} d\ell + t_a^2\int_{\ell=0}^{\ell_m} d\ell\right] \tag{G2}$$

since the weight is

$$W_m = \rho_T \mathscr{V} \tag{G3}$$

Substituting equation (G2) into (G3) and integrating yield

$$W_m = \rho_T \pi t_a \ell_m\left[\frac{4}{3}\left(\frac{\dot{\mathscr{M}}_0}{\rho\pi V}\right)^{1/2} + t_a\right] \tag{G4}$$

When $\dot{\mathscr{M}}_0$ is replaced with the proper equivalent, the manifold weights are

$$W_{m,g} = 2\rho_T \pi t_a \ell_m\left[\frac{4}{3}\left(\frac{\dot{M}}{2\rho_g \pi V_g}\right)^{1/2} + t_a\right] \tag{G5}$$

and

$$W_{m,f} = N_p \rho_T \pi t_a \ell_m\left[\frac{4}{3}\left(\frac{\dot{M}}{N_p \rho_f \pi V_f}\right)^{1/2} + t_a\right] \tag{G6}$$

APPENDIX H

ANGLE FACTORS

The angle factor for the heat emission from a differential element of the fin to the tube has been derived as a general case in reference 18. Given two surfaces, one of differential size and the other a cylindrical surface of arbitrary profile, whose generating lines are parallel to the first surface, shown in sketch (c), it was shown that the angle factor of the cylindrical surface A_2 from the differential element dA_1 is

$$F_{dA_1,2} = \frac{1}{2}(\sin \Phi' - \sin \Phi'') \tag{H1}$$

For the fin and tube geometry of the radiator $\Phi' = \pi/2$. The angle factors from the differential element of the fin de to the tube surfaces designated 1 and 2 in sketch (d) are

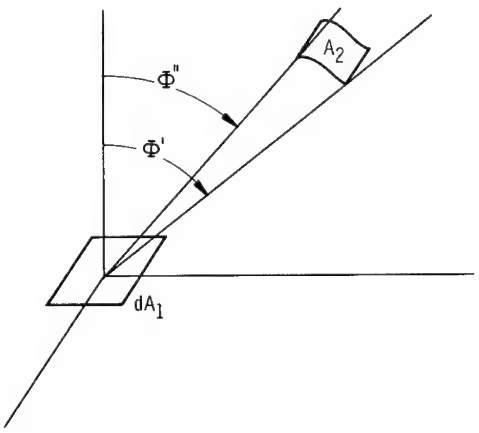

(c)

$$F_{de,1} = \frac{1}{2}(1 - \cos \Phi_1) \tag{H2}$$

and

$$F_{de,2} = \frac{1}{2}(1 - \cos \Phi_2) \tag{H3}$$

For this study, the interradiation between the fin and the tube was neglected and only the radiation to space considered. Thus,

$$F_{de,space} = 1 - F_{de,1} - F_{de,2} = \frac{1}{2}(\cos \Phi_1 + \cos \Phi_2) \tag{H4}$$

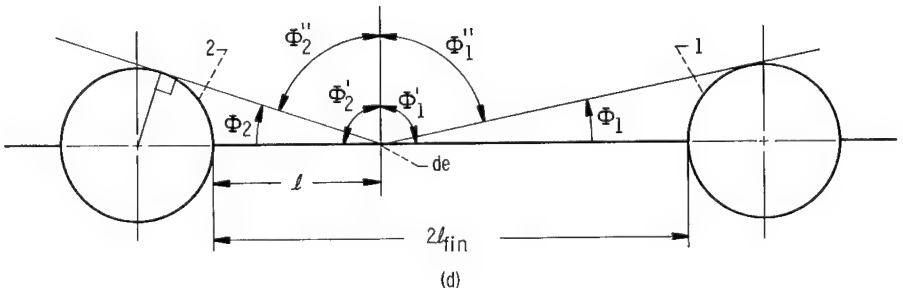

(d)

The angle factors from $\ell = 0$ to $\ell = \ell_{fin}$ were found in increments and a mean value was calculated by using the trapezoidal rule:

$$F_{fin} = \frac{\sum_{n=1}^{n=\ell_{fin}/\Delta\ell} \frac{1}{2}\left[\left(F_{de,space}\right)_{n-1} + \left(F_{de,space}\right)_{n}\right]\Delta\ell}{\ell_{fin}} \tag{H5}$$

The angle factor from any point on the tube to the fin and adjacent tube is found similarly. Here the differential element (see sketch (e)) lies on the tube and the cylindrical surface is the fin surface plus part of the adjacent tube:

$$F_{d\psi,1} = \frac{1}{2}(1 - \cos\Omega) \tag{H6}$$

For emission directly to space,

$$F_{d\psi,space} = 1 - F_{d\psi,1} = \frac{1}{2}(1 + \cos\Omega) \tag{H7}$$

The relation between Ω and ψ is shown in reference 19 to be

$$\cos\Omega = \frac{C\sin\psi\sqrt{C^2 - 2C\cos\psi} - (C\cos\psi - 1)}{C^2 - 2C\cos\psi + 1} \tag{H8}$$

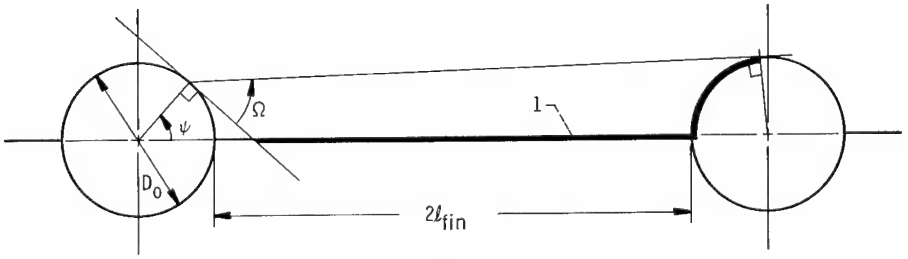

(e)

where

$$C = 2\left(1 + \frac{2\ell_{fin}}{D_o}\right) \tag{H9}$$

The mean value of the tube angle factor for $0 \leq \psi \leq \pi/2$ was obtained numerically by using the trapezoidal rule:

$$F_t = \frac{\sum_{n=1}^{n=\frac{\pi/2}{\Delta\psi}} \frac{1}{2}\left[\left(F_{d\psi,\,space}\right)_{n-1} + \left(F_{d\psi,\,space}\right)_n\right]\Delta\psi}{\pi/2} \tag{H10}$$

REFERENCES

1. Ross, D.P.; Ray, E.; and Haller, H.C.: Heat Rejection from Space Vehicles. Paper No. 60-39, AAS, Jan. 1960.

2. Holden, P.C.; and Stump, F.C.: Optimized Condenser-Radiator for Space Applications. Paper No. 60-AV-16, ASME, June 1960.

3. Denington, R.J.; Koestel, A.; Saule, A.V.; Shure, L.I.; Stevens, G.T.; and Taylor, R.B.: Space Radiator Study. Rept. No. TR 61-697, Air Force Systems Command, Oct. 1963.

4. Krebs, Richard P.; Winch, David M.; and Lieblein, Seymour: Analysis of a Megawatt Level Direct Condenser-Radiator. Progress in Astronautics and Aeronautics. Vol. 11 - Power Systems for Space Flight. Academic Press, Inc., 1963, pp. 475-504.

5. Anderson, R.C.; and Henderson, B.J.: A Parametric Survey of Tube and Fin Type Radiators. Rept. No. LAMS-2793, Los Alamos Sci. Lab., Oct. 1962.

6. Stone, R.; and Coombs, M.G.: Large Space Radiators. Paper Presented at Propulsion Meeting, IAS, Cleveland (Ohio), Mar. 7-8, 1963.

7. English, Robert E.; and Guentert, Donald C.: Segmenting of Radiators for Meteoroid Protection. ARS J., vol. 31, no. 8, Aug. 1961, pp. 1162-1164.

8. Moffitt, Thomas P.; and Klag, Frederick W.: Analytical Investigation of Cycle Characteristics for Advanced Turboelectric Space Power Systems. NASA TN D-472, 1960.

9. Mackay, D.B.; and Bacha, C.P.: Space Radiator Analysis and Design, Pt. I. Rept. No. TR 61-30 (SID 61-66), Aeronaut. Systems Div., Apr. 1, 1961.

10. Haller, Henry C.; Wesling, Gordon C.; and Lieblein, Seymour: Heat-Rejection and Weight Characteristics of Fin-Tube Space Radiators with Tapered Fins. NASA TN D-2168, 1964.

11. Loeffler, I.J.; Lieblein, Seymour; and Clough, Nestor: Meteoroid Protection for Space Radiators. Vol. 11 - Progress in Astronautics and Aeronautics. Power Systems for Space Flight. Academic Press, Inc., 1963, pp. 551-579.

12. Davison, Elmer H.; and Winslow, Paul C., Jr.: Space Debris Hazard Evaluation. NASA TN D-1105, 1961.

13. Lieblein, Seymour: Analysis of Temperature Distribution and Radiant Heat Transfer Along a Rectangular Fin of Constant Thickness. NASA TN D-196, 1959.

14. Fauske, Hans K.: Contribution to the Theory of Two-Phase, One-Component Critical Flow. Rept. No. ANL-6633 (TID-4500, 18th ed.), Argonne Nat. Lab., Oct. 1962.

15. Weatherford, W.D., Jr.; Tyler, John C.; and Ku, P.M.: Properties of Inorganic Energy-Conversion and Heat-Transfer Fluids for Space Applications. Rept. No. TR 61-96, WADD, Nov. 1961.

16. McAdams, W.H.: Heat Transmission. Third ed., McGraw-Hill Book Co., Inc., 1954.

17. Lockhart, R.W.; and Martinelli, R.C.: Proposed Correlation of Data for Isothermal Two-Phase, Two-Component Flow in Pipes. Chem. Eng. Prog., vol. 45, no. 1, Jan. 1949, pp. 39-45; Discussion, pp. 45-48.

18. Jakob, Max: Heat Transfer. Vol. II. John Wiley & Sons, Inc., 1959.

19. Callinan, Joseph P.; and Berggren, Willard P.: Some Radiator Design Criteria for Space Vehicles. J. Heat Transfer (ASME Trans.), ser. C, vol. 81, no. 3, Aug. 1959, pp. 237-244.

NASA-Langley, 1966 E-2472

"The aeronautical and space activities of the United States shall be conducted so as to contribute . . . to the expansion of human knowledge of phenomena in the atmosphere and space. The Administration shall provide for the widest practicable and appropriate dissemination of information concerning its activities and the results thereof."

—NATIONAL AERONAUTICS AND SPACE ACT OF 1958

NASA SCIENTIFIC AND TECHNICAL PUBLICATIONS

TECHNICAL REPORTS: Scientific and technical information considered important, complete, and a lasting contribution to existing knowledge.

TECHNICAL NOTES: Information less broad in scope but nevertheless of importance as a contribution to existing knowledge.

TECHNICAL MEMORANDUMS: Information receiving limited distribution because of preliminary data, security classification, or other reasons.

CONTRACTOR REPORTS: Technical information generated in connection with a NASA contract or grant and released under NASA auspices.

TECHNICAL TRANSLATIONS: Information published in a foreign language considered to merit NASA distribution in English.

TECHNICAL REPRINTS: Information derived from NASA activities and initially published in the form of journal articles.

SPECIAL PUBLICATIONS: Information derived from or of value to NASA activities but not necessarily reporting the results of individual NASA-programmed scientific efforts. Publications include conference proceedings, monographs, data compilations, handbooks, sourcebooks, and special bibliographies.

Details on the availability of these publications may be obtained from:

SCIENTIFIC AND TECHNICAL INFORMATION DIVISION

NATIONAL AERONAUTICS AND SPACE ADMINISTRATION

Washington, D.C. 20546